custEM: From open-source 3D EM modeling towards inversion

EMinar

March 16, 2022

Raphael Rochlitz

with contributions of Thomas Günther, the DESMEX Team
and several members of the EM community

Flat-surface EM geometries

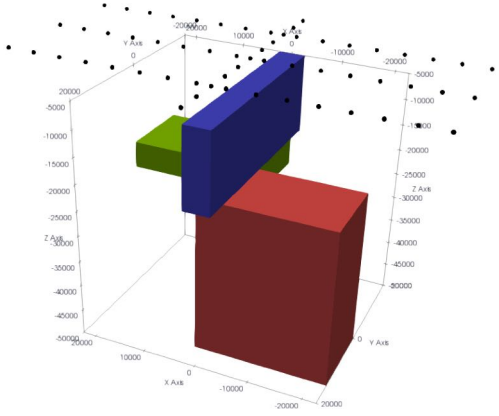

Flat-surface EM geometries

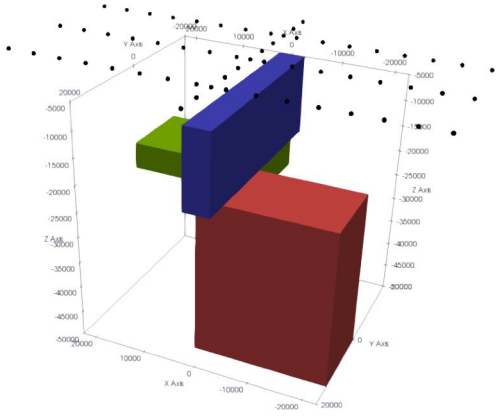

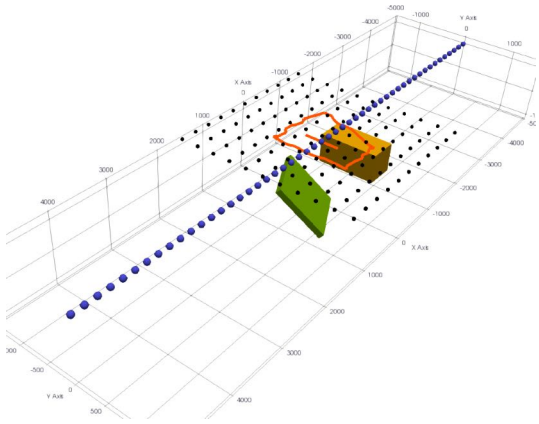

Complex real-world EM geometries

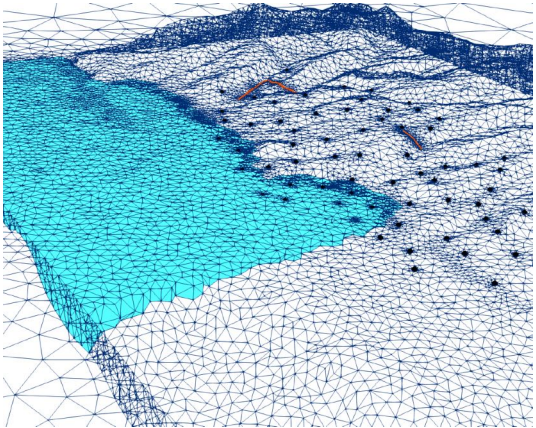

Complex real-world EM geometries

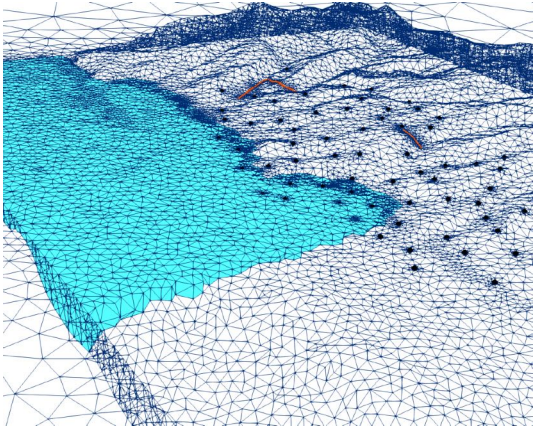

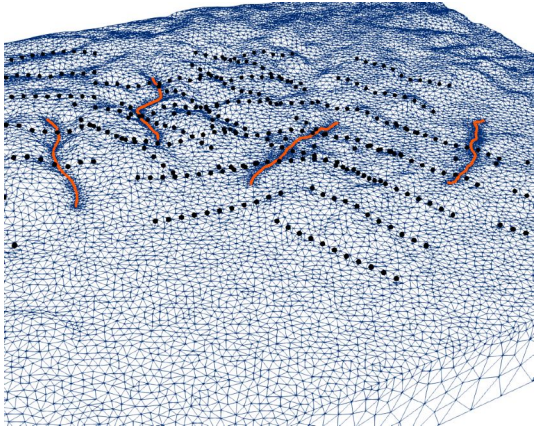

Outline

- Motivation
- EM modeling
- CSEM inversion
- custEM

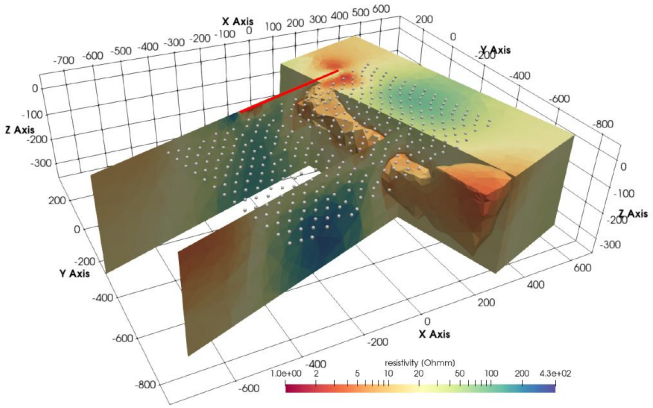

State of research (2017) in 3D geophysical EM modeling

	MT	CSEM	TEM
integral equation	(Ting and Hohmann, 1981), (Wannamaker, 1991), (Kruglyakov et al., 2016)	(Raiche, 1974), (Weidelt et al., 1975), (Hohmann, 1975), (Zhdanov et al., 2006)	(SanFilipo and Hohmann, 1985), (Hohmann, 1983), (Slob et al., 1999)
finite difference	(Mackie and Madden, 1993), (Siripunvaraporn et al., 2002), (Kelbert et al., 2014)	(Alumbaugh et al., 1996), (Commer and Newman, 2004), (Streich, 2009)	(Druskin and Knizhnerman, 1988), (Adhidjaja and Hohmann, 1989), (Wang and Hohmann, 1993)
finite volume	(Madden and Mackie, 1989)	(Haber et al., 2000), (Jahandari and Farquharson, 2014)	(Haber et al., 2002)
finite element	(Mitsuhata and Uchida, 2004), (Farquharson and Miensopust, 2011), (Ren et al., 2013), (Grayver and Bürg, 2014), (Kordy et al., 2017)	(Coggon, 1971), (Biro and Preis, 1989), (Pridmore et al., 1981; Gupta et al., 1989; Livelybrooks, 1993), (Badea et al., 2001; Stalnaker, 2005; Puzyrev et al., 2013; Tang et al., 2015), (Schwarzbach, 2009; Schwarzbach et al., 2011; Da Silva et al., 2012; Cai et al., 2014; Mukherjee and Everett, 2011), (Ansari and Farquharson, 2014; Ansari, 2014; Li et al., 2016b,a)	(Um et al., 2010), (Um et al., 2012), (Börner et al., 2015), (Cai et al., 2017)

Multiple EM methods jointly applied

CSAMT MT CSEM TEM LOTEM AFMAG

Separate codes for the simulation of CSEM, TEM or MT data?

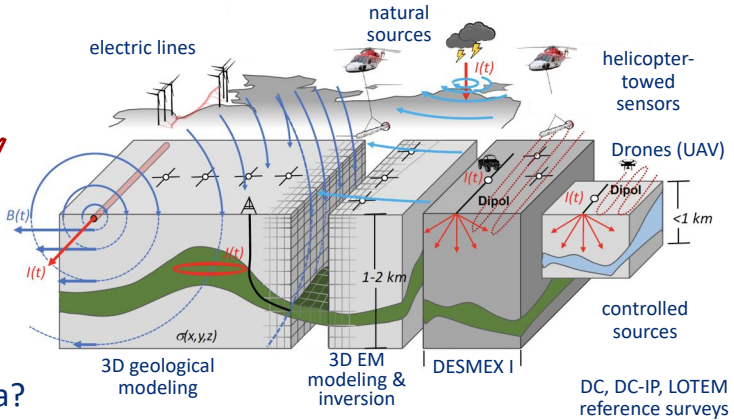

Geophysical EM modeling

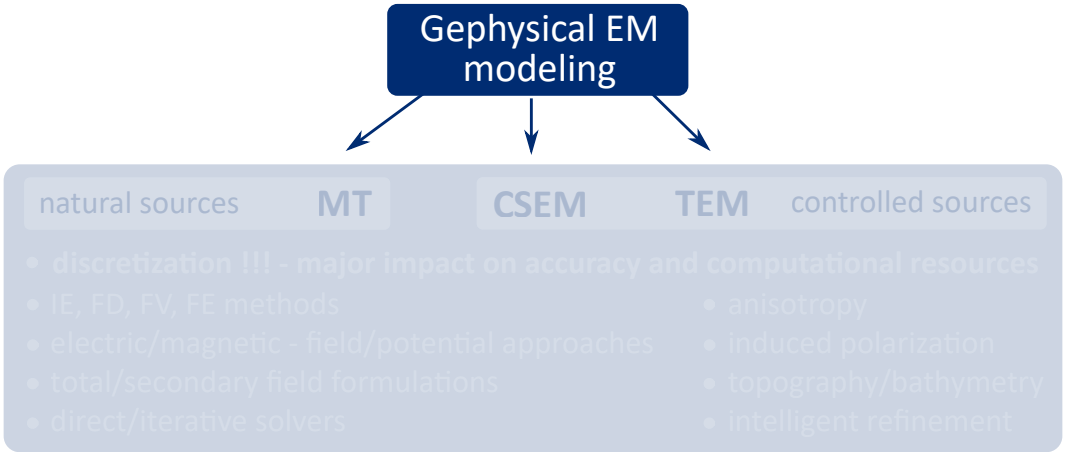

Geophysical EM modeling

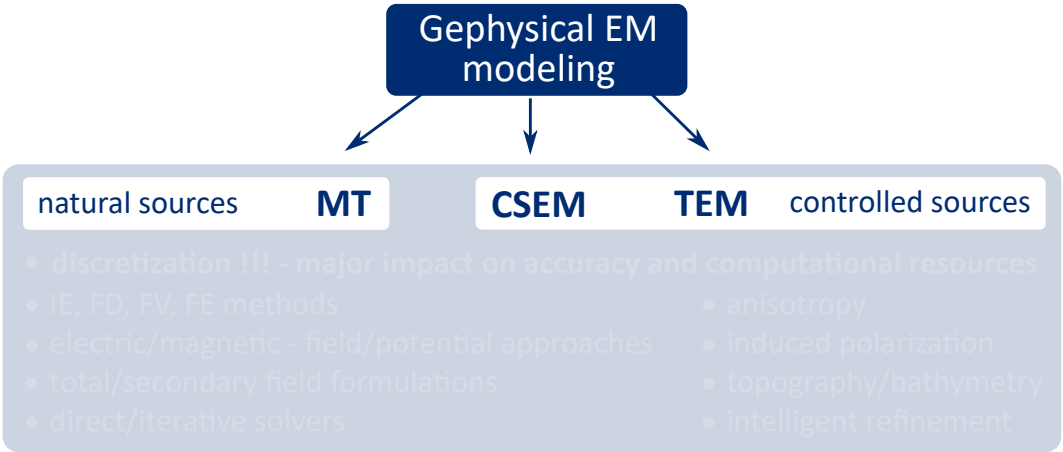

Geophysical EM modeling

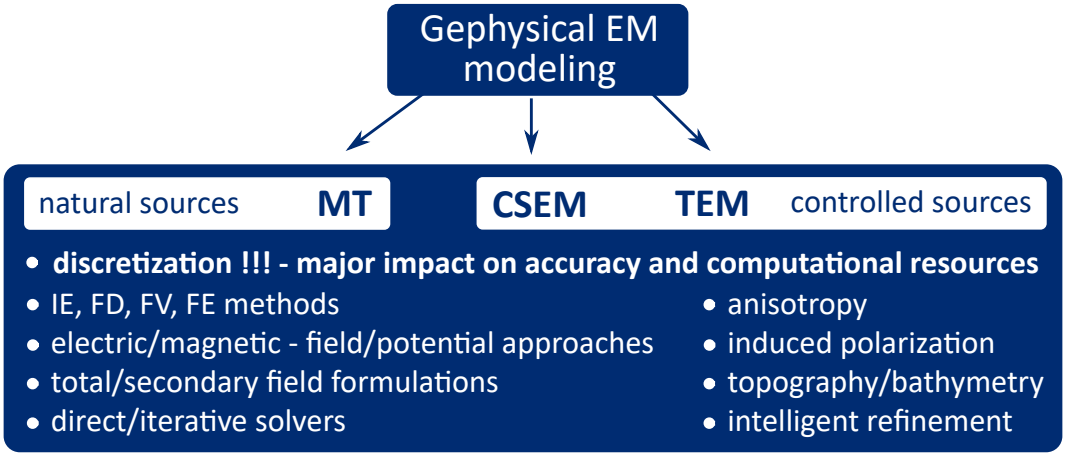

Recent development of 3D EM modeling

- impact of individual developments
- innovation
- publications
- redundancy
- detailed error analysis
- availability

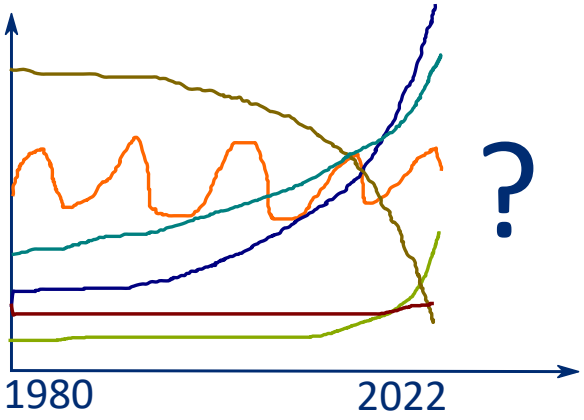

MTnet - list of available source codes

1D Codes

- 1D anisotropy forward code (from Xiaobo Li) Compressed zip file, 54 Kb
- Rho+ code: (from Bob Parker and John Booker) Compressed zip, 64 Kb (Version 2.0: 18-05-97)
- Occam 1D code: home page (from Steve Constable)
- IPI2win_MT: Windows-based 1D automatic and manual interpretation code (from Alexei Bobatchev)

Back to top

2D Codes

- NFEM2D from Ralph-Uwe Boerner
- Occam 2D code: home page (from Steve Constable)
- Occam 2D sharp boundary code: home page (from Catherine deGroot-Hedlin)
- RRI: rapid relaxation inversion (from John Booker, Torquil Smith & Nong Wu)
- REBOCC: Weerachai Siripunvaraporn and Gary Egbert's 2D inversion code
  - Information
  - Send an email to Weerachai Siripunvaraporn
- MT2D: A c++ based 2D magnetotellurics and radio-magnetotellurics finite element solver using unstructrued grids (from Zhengyong Ren)

Back to top

3D Codes

- Klaus Spitzer's 3D DC & IP forward modelling codes for surface and borehole applications:
  - 3DDC: version 4.3
  - 3DDCXH: version 6.3
  - 3DIPXH: version 2.3

  Codes include grid-independent electrode positioning.
  Send an email to Klaus Spitzer
- WSINV3DMT: Weerachai Siripunvaraporn's 3D MT inversion code
- ModEM: Modular EM Inversion Software (from Gary Egbert, Anna Kelbert and Naser Meqbel)

Back to top

More and more "open-source" developments

Overview with no claim of completeness! There are probably way more (in particular, MT and 1D/2D) tools freely available (or on request)

ModEM Geophysics
Innovating solutions in EM Geophysics

Kelbert et al. (2014)

WSINV3DMT

Siripunvaraporn and Egbert (2009)

GoFEM

Grayver et al. (2019)

Werthmüller et al. (2021)

emtmod

Werthmüller (2017)

MARE2DEM

Key (2016)

simpeg

Cockett et al. (2015)

emg3d

POLYEM3D

Bretaudeau et al. (2017)

+1D/2D codes on MTnet

petgem

Castillo-Reyes et al. (2018)

custEM

Rochlitz et al. (2019)

Approaches

Total field (TF) formulations

Secondary field (SF) formulations

E-field approach: e.g. Schwarzbach (2009); Grayver and Bürg (2014)

$$\mathbf{E} = \mathbf{E^s} + \mathbf{E^0}$$

$$\nabla \times \mu^{-1} \nabla \times \mathbf{E} + i\omega\sigma\mathbf{E} = -i\omega\mathbf{j_e}$$

$$\nabla \times \mu^{-1} \nabla \times \mathbf{E^s} + i\omega\sigma\mathbf{E^s} = -i\omega\Delta\sigma\mathbf{E^0}$$

H-field approach:

$$\mathbf{E} = \tfrac{1}{\sigma} \nabla \times \mathbf{H}$$

$$\Delta\sigma = \sigma - \sigma_0$$

$$\nabla \times \sigma^{-1} \nabla \times \mathbf{H} + i\omega\mu\mathbf{H} = \nabla \times \sigma^{-1}\,\mathbf{j_e}$$

$$\nabla \times \sigma^{-1} \nabla \times \mathbf{H^s} + i\omega\mu\mathbf{H^s} = \nabla \times \Delta\rho \nabla \times \mathbf{H^0}$$

A-Φ approaches:

$$\mathbf{H} = (i\omega\mu)^{-1} \nabla \times \mathbf{E}$$

$$\mathbf{H} = \mu^{-1} \nabla \times \mathbf{A} \qquad \mathbf{E} = -i\omega\mathbf{A} - \nabla\Phi$$

$$\nabla \times \nabla \times \mathbf{A} + i\omega\mu\sigma\mathbf{A} + \mu\sigma\nabla\Phi = \mu\mathbf{j_e}$$

$$i\omega\nabla \cdot (\sigma\mathbf{A}) + \nabla \cdot (\sigma\nabla\Phi) = -\nabla \cdot \mathbf{j_e}$$

$$\nabla \times \nabla \times \mathbf{A^s} + i\omega\mu\sigma\mathbf{A^s} + \mu\sigma\nabla\Phi^s = i\omega\mu\Delta\sigma\mathbf{A^0}$$

$$i\omega\nabla \cdot (\sigma\mathbf{A^s}) + \nabla \cdot (\sigma\nabla\Phi^s) = -i\omega\nabla \cdot (\Delta\sigma\mathbf{A^0})$$

3 TF and 5 SF approaches implemented in *custEM*, **E** and **H** can be calculated with all approaches

- More details: Rochlitz et al. (2019), Rochlitz (2020)

Halfspace model - discretization

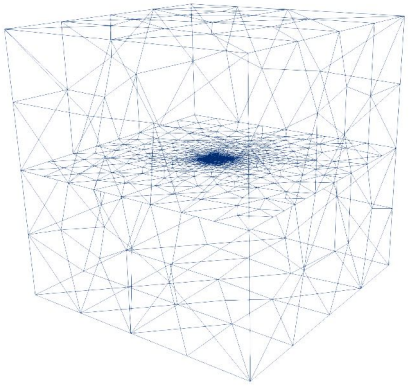

- 1 m x-directed HED Tx
- 101 Rx on oblique observation line
- 1, 10, 100, & 1000 Hz
- airspace: 1e8 Ωm
- subsurface: 1e2 Ωm
- reference solution: empymod Werthmüller (2017)

Halfspace model - discretization

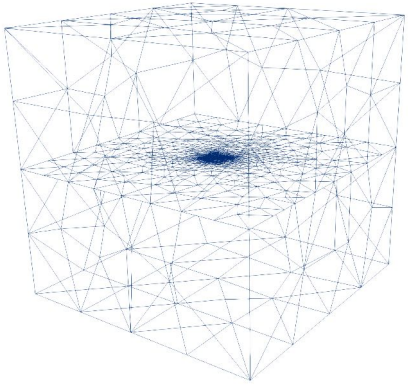

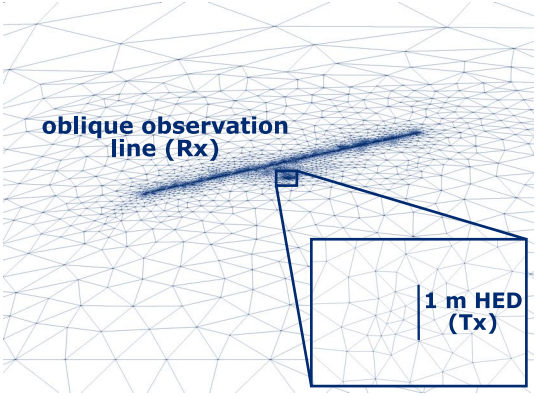

Halfspace model - discretization

Refinement characteristics

p1
ℓ = 1 m, q = 1.2

p2
ℓ = 20 m, q = 1.4

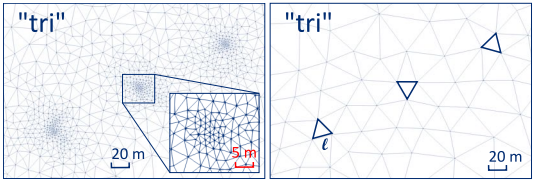

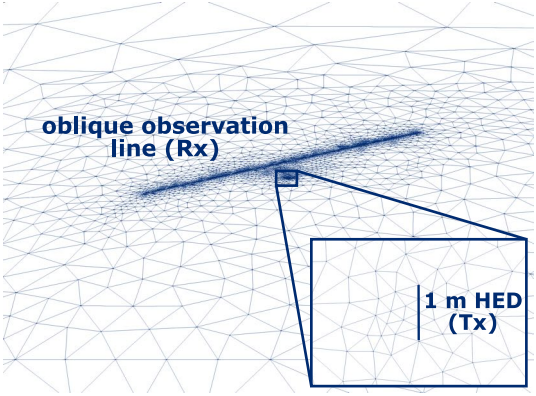

Halfspace model - accuracy of first and second order polynomials

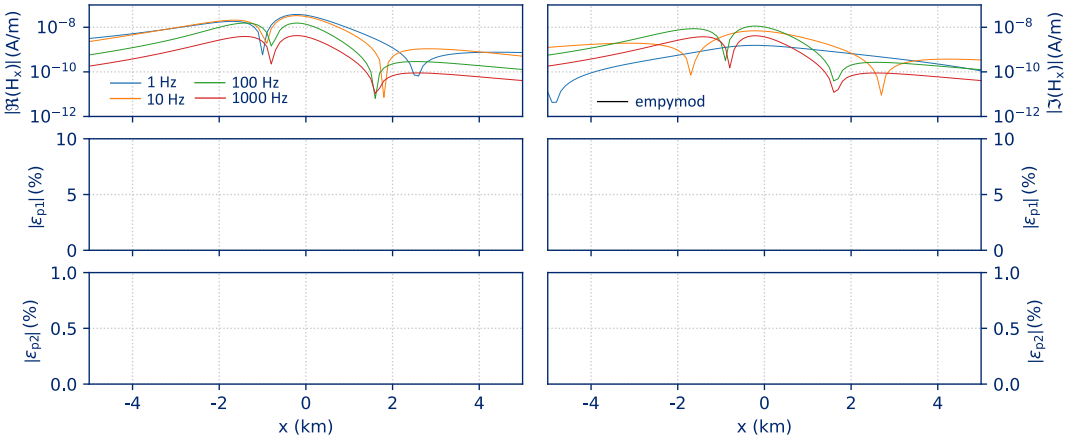

Halfspace model - accuracy of first and second order polynomials

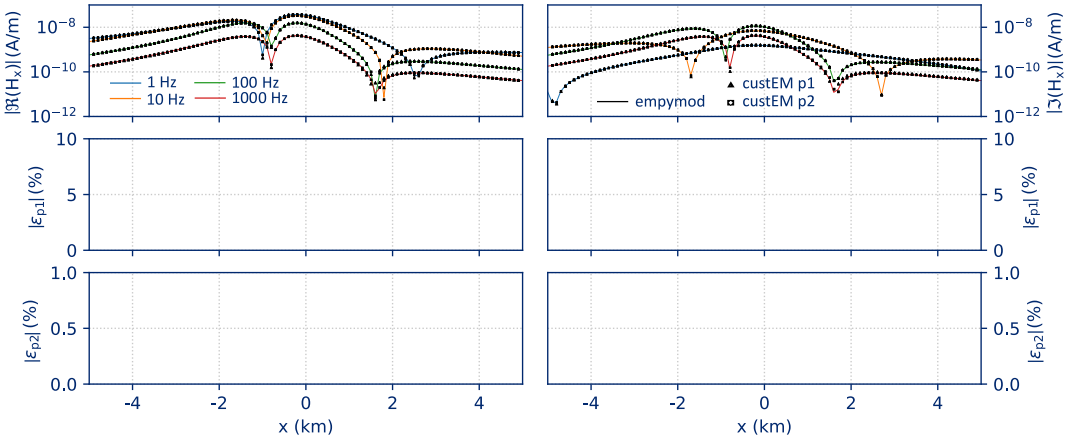

Halfspace model - accuracy of first and second order polynomials

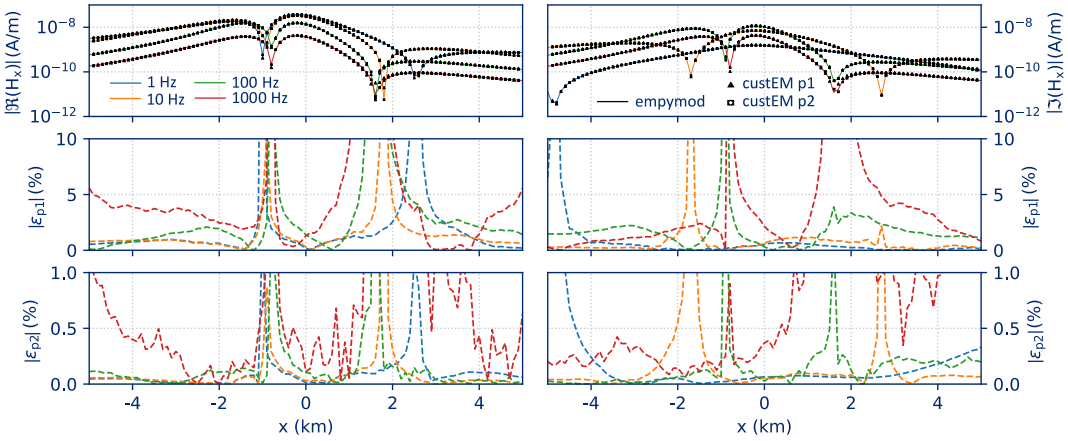

Computational performance

Table: Computational performance of p1 and p2 - halfspace model

mesh	l(m)	q	order	dof (M)	RAM (GB)	CT (s)
fine	1	1.2	p1	1.9	≈50	≈22
coarse	20	1.4	p2	0.84	≈50	≈26

Modeling examples including variable physical parameters

- Full anisotropy: Wang et al. (2022)
- Magnetic permeability: Rulff et al. (2021)
- Induced polarization, 1D validation of 3-layer model against empymod, model details and errors in Appendix

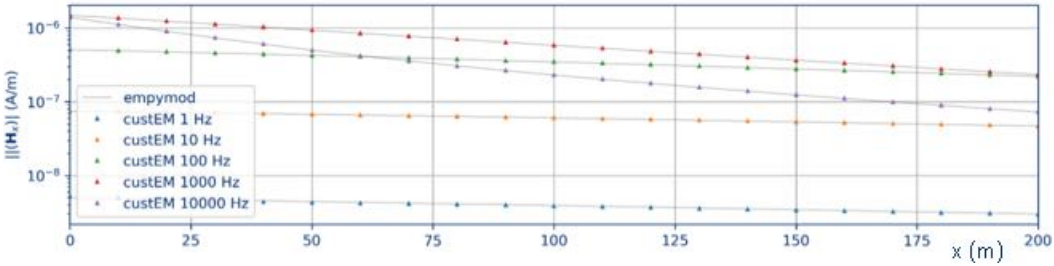

Marlim R3D - marine hydrocarbon reference model

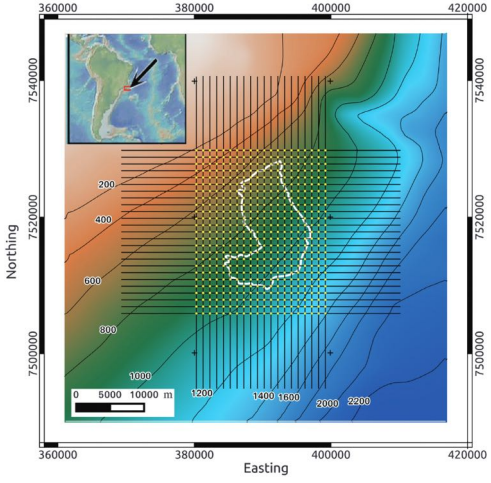

Correa and Menezes (2019)

Marlim R3D - marine hydrocarbon reference model

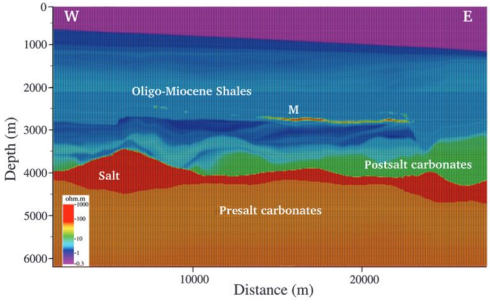

Figure 3. Cross section of the MR3D vertical resistivity along the east–west towline 04Tx013. Marlim oil-prone turbidites (M) appear as thin resistive bodies.

Correa and Menezes (2019)

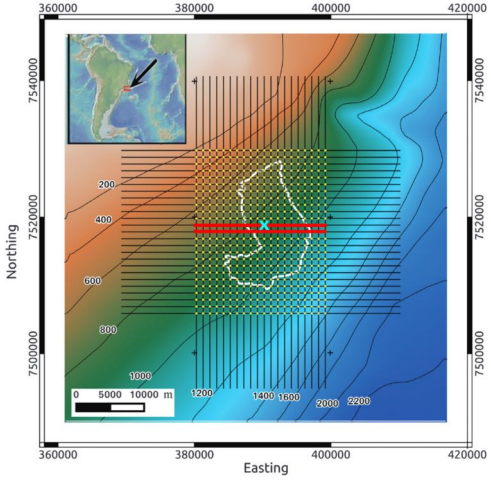

Marlim R3D - marine hydrocarbon reference model

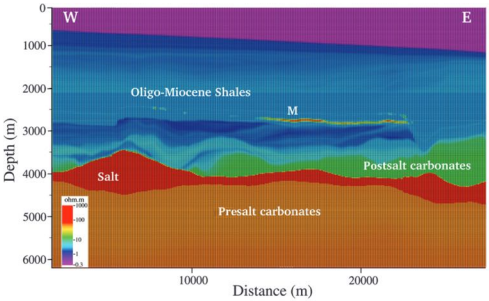

Figure 3. Cross section of the MR3D vertical resistivity along the east–west towline 04Tx013. Marlim oil-prone turbidites (M) appear as thin resistive bodies.

Correa and Menezes (2019)

Constraining lithological horizons using interface-information from reflection seismic surveys

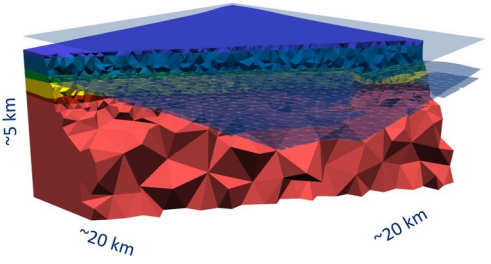

Marlim R3D - interpolating resistivities

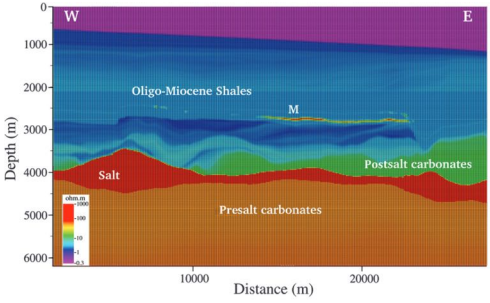

Figure 3. Cross section of the MR3D vertical resistivity along the east–west towline 04Tx013. Marlim oil-prone turbidites (M) appear as thin resistive bodies.

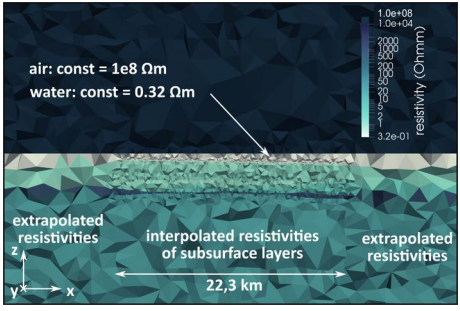

interpolated resistivities on custEM mesh

Marlim R3D - Results from Werthmüller et al. (2020)

Werthmüller, Rochlitz, Castillo-Reyes, Heagy, 2021, *Open source landscape in CSEM modeling*

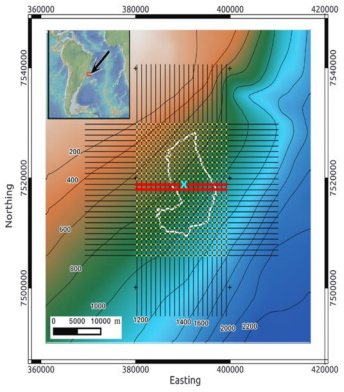

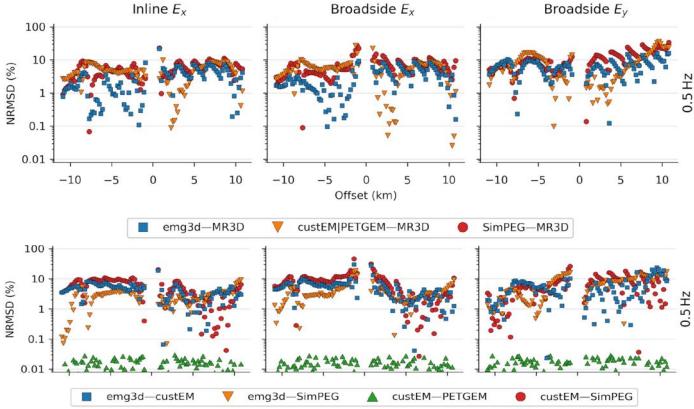

Time-domain modeling approaches

$$\nabla \times \mu^{-} \nabla \times \mathbf{E} + i\omega\sigma\mathbf{E} = -i\omega\mathbf{j}_e$$

frequency domain

inverse FT

1. FT-based methods

$$\nabla \times \mu^{-1} \nabla \times \mathbf{e} + \sigma \frac{\partial \mathbf{e}}{\partial t} = -\frac{\partial \mathbf{j}_e^t}{\partial t}$$

time domain

Δt

2. Implicit Euler method

matrix exponentials

3. Rational Arnoldi method

More details: Rochlitz, R., Seidel, M., Börner, R.-U. (2021), GJI.

LOTEM comparison model

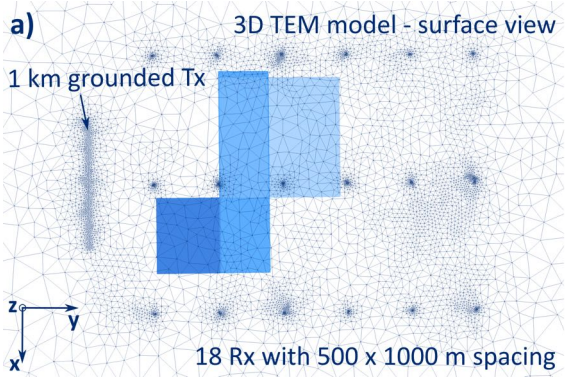

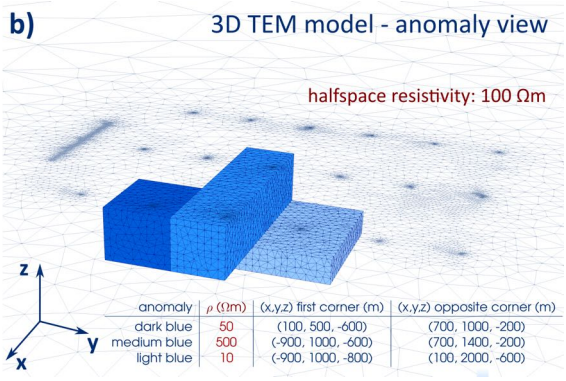

anomaly	ρ (Ωm)	(x,y,z) first corner (m)	(x,y,z) opposite corner (m)
dark blue	50	(100, 500, -600)	(700, 1000, -200)
medium blue	500	(-900, 1000, -600)	(700, 1400, -200)
light blue	10	(-900, 1000, -800)	(100, 2000, -600)

LOTEM comparison of three custEM methods and SLDMEM (Uni Cologne)

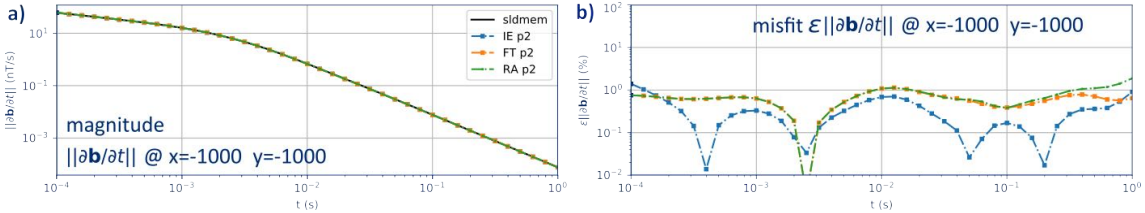

- FT method: 120 min → depends on FHT coefficients (here 80)
- IE method: 20 min → depends on time stepping
- RA method: 2 min → simply very fast

MT modeling - Dublin Test model 1 (Miensopust, 2017)

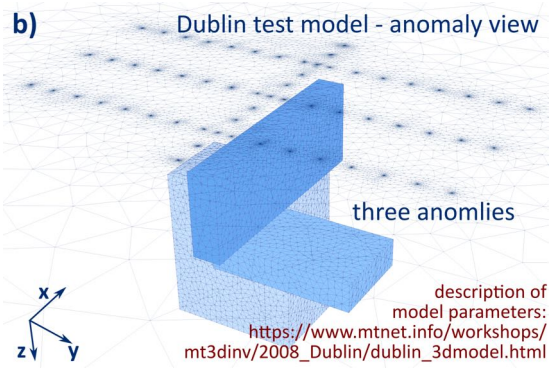

MT modeling - Dublin Test model 1 (Miensopust, 2017)

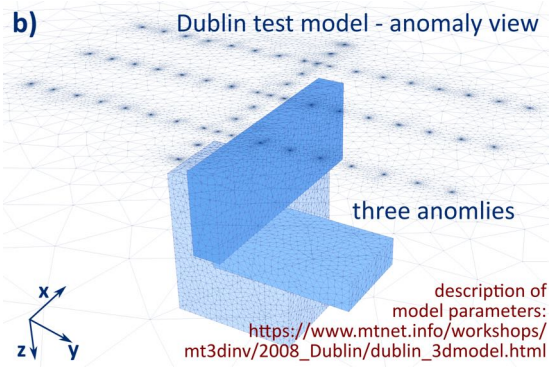

description of model parameters: https://www.mtnet.info/workshops/mt3dinv/2008_Dublin/dublin_3dmodel.html

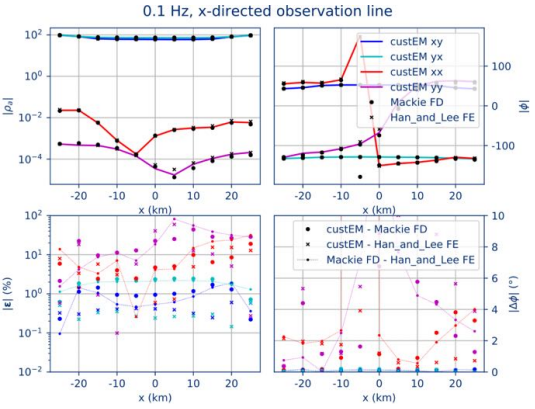

Outlook - 3D EM modeling

2022 → 2032

- Iterative solver/preconditioner for total E-field approach (save RAM!)
- Better accuracy! Mismatches of $> 1\%$ in many benchmark studies not satisfying
- More irregular community models suited for benchmarking unstructured-grid codes

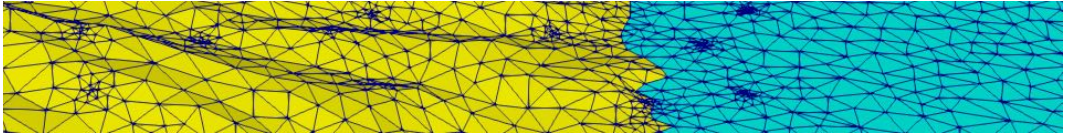

Deep Electromagnetic Sounding for Mineral EXploration

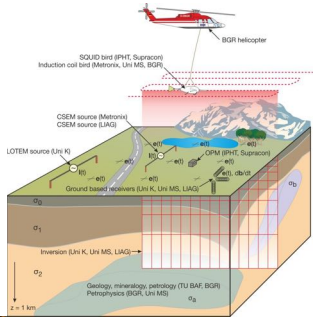

Inversion methodology

Rücker et al. (2017)

Minimize objective function

$$||\mathbf{W}_\mathrm{d}\left(\mathscr{F}\left(\mathbf{m}\right)-\mathbf{d}\right)||_2^2+\lambda||\mathbf{W}_\mathrm{m}\left(\mathbf{m}-\mathbf{m}_0\right)||_2^2\rightarrow\min$$

Gauss-newton scheme

$$\left(\mathbf{J}^\mathrm{T}\mathbf{W}_\mathbf{d}^\mathrm{T}\mathbf{W}_\mathbf{d}\mathbf{J}+\lambda\mathbf{W}_\mathbf{m}^\mathrm{T}\mathbf{W}_\mathbf{m}\right)\Delta\mathbf{m}^k=\mathbf{J}^\mathrm{T}\mathbf{W}_\mathbf{d}^\mathrm{T}\mathbf{W}_\mathbf{d}\left(\Delta\mathbf{d}^k\right)$$
$$-\lambda\mathbf{W}_\mathbf{m}^\mathrm{T}\mathbf{W}_\mathbf{m}\left(\mathbf{m}^k-\mathbf{m}^0\right)$$
$$\text{with}\quad\Delta\mathbf{d}^k=\mathbf{d}-\mathscr{F}\left(\mathbf{m}^k\right)\quad\text{and}\quad\Delta\mathbf{m}^k=\mathbf{m}^k-\mathbf{m}^{k-1}$$

custEM

Inversion methodology

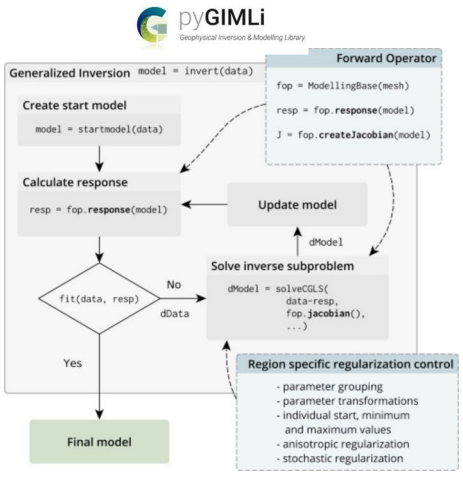

Rücker et al. (2017)

Minimize objective function

$$||\mathbf{W}_\mathrm{d}\left(\mathscr{F}\left(\mathbf{m}\right)-\mathbf{d}\right)||_2^2+\lambda||\mathbf{W}_\mathrm{m}\left(\mathbf{m}-\mathbf{m}_0\right)||_2^2\rightarrow\min$$

Gauss-newton scheme

$$\left(\mathbf{J}^\mathrm{T}\mathbf{W}_\mathbf{d}^\mathrm{T}\mathbf{W}_\mathbf{d}\mathbf{J}+\lambda\mathbf{W}_\mathbf{m}^\mathrm{T}\mathbf{W}_\mathbf{m}\right)\Delta\mathbf{m}^k=\mathbf{J}^\mathrm{T}\mathbf{W}_\mathbf{d}^\mathrm{T}\mathbf{W}_\mathbf{d}\left(\Delta\mathbf{d}^k\right)-\lambda\mathbf{W}_\mathbf{m}^\mathrm{T}\mathbf{W}_\mathbf{m}\left(\mathbf{m}^k-\mathbf{m}^0\right)$$

$$\text{with}\quad\Delta\mathbf{d}^k=\mathbf{d}-\mathscr{F}\left(\mathbf{m}^k\right)\quad\text{and}\quad\Delta\mathbf{m}^k=\mathbf{m}^k-\mathbf{m}^{k-1}$$

custEM

Explicit sensitivity calculations

E.g., Rodi (1976); Egbert and Kelbert (2012); Grayver et al. (2013); Wang et al. (2018)

The Jacobian:

$$\mathrm{J_{i,j}} = \frac{\partial d_i}{\partial m_j}, \quad i = 1 \ldots N, \quad j = 1 \ldots M.$$

$$\mathbf{J} = \begin{pmatrix} \mathbf{J}_1 \\ \vdots \\ \mathbf{J}_k \\ \vdots \\ \mathbf{J}_{N_f} \end{pmatrix}, \qquad \mathbf{J}_k = \begin{pmatrix} \mathbf{J}_{k,\mathrm{E}} \\ \mathbf{J}_{k,\mathrm{H}} \end{pmatrix},$$

shape of $\mathbf{J}_k$: $2 * N_{obs} * N_s$

Map $\mathbf{F}$ ($\mathbf{E}$ or $\mathbf{H}/\mathbf{B}$) with interpolation matrices:

$$\mathbf{f}(\mathrm{m})_\mathrm{F} = \mathbf{Q}\mathbf{F}\,.$$

Re-use system matrix factorization:

$$\mathbf{J}_{k,\mathrm{F}} = \mathbf{Q}\mathbf{A}_\mathrm{F}^{-1}\mathbf{G}_\mathrm{F}\,.$$

with

$$\mathbf{G}_\mathrm{F} = \{\partial \mathbf{b}_\mathrm{F}/\partial m_1,\ \partial \mathbf{b}_\mathrm{F}/\partial m_2,\ \ldots,\ \partial \mathbf{b}_\mathrm{F}/\partial m_M\}\,.$$

Use reciprocity trick:

$$\mathbf{J}_{k,\mathrm{F}}^T = \mathbf{Q}^T\mathbf{A}_\mathrm{F}^{-1}\mathbf{G}_\mathrm{F}^T\,,$$

Explicit sensitivity calculations

E.g., Rodi (1976); Egbert and Kelbert (2012); Grayver et al. (2013); Wang et al. (2018)

The Jacobian:

$$\mathrm{J_{i,j}} = \frac{\partial d_i}{\partial m_j}, \quad i = 1 \dots N, \quad j = 1 \dots M.$$

$$\mathbf{J} = \begin{pmatrix} \mathbf{J}_1 \\ \vdots \\ \mathbf{J}_k \\ \vdots \\ \mathbf{J}_{N_f} \end{pmatrix}, \qquad \mathbf{J}_k = \begin{pmatrix} \mathbf{J}_{k,\mathrm{E}} \\ \mathbf{J}_{k,\mathrm{H}} \end{pmatrix},$$

shape of $\mathbf{J}_k$: $2 * N_{obs} * N_s$

Map $\mathbf{F}$ ($\mathbf{E}$ or $\mathbf{H}/\mathbf{B}$) with interpolation matrices:

$$\mathbf{f}(\mathrm{m})_{\mathrm{F}} = \mathbf{Q}\mathbf{F}\,.$$

Re-use system matrix factorization:

$$\mathbf{J}_{k,\mathrm{F}} = \mathbf{Q}\mathbf{A}_{\mathrm{F}}^{-1}\mathbf{G}_{\mathrm{F}}\,.$$

with

$$\mathbf{G}_{\mathrm{F}} = \{\partial \mathbf{b}_{\mathrm{F}}/\partial m_1,\ \partial \mathbf{b}_{\mathrm{F}}/\partial m_2,\ \dots,\ \partial \mathbf{b}_{\mathrm{F}}/\partial m_M\}\,.$$

Use reciprocity trick:

$$\mathbf{J}_{k,\mathrm{F}}^{T} = \mathbf{Q}^{T}\mathbf{A}_{\mathrm{F}}^{-1}\mathbf{G}_{\mathrm{F}}^{T}\,,$$

Mesh design - 2.5D inversion

For inversion of "line data", cross-comparison with established MARE2DEM (Key, 2016)

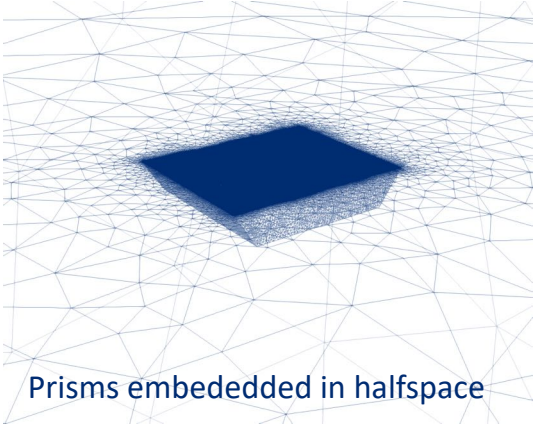

Prisms embededdedded in halfspace

Inner mesh

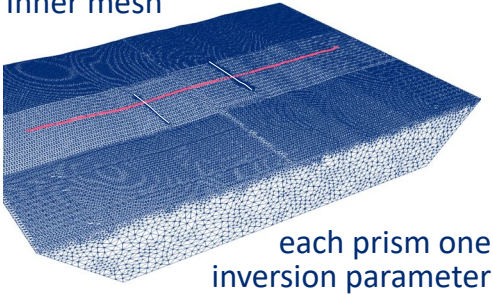

each prism one inversion parameter

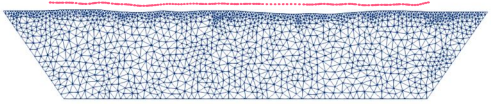

Mesh design - 3D inversion

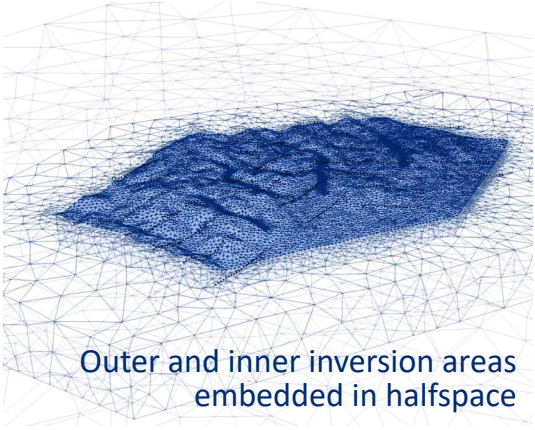

Outer and inner inversion areas embedded in halfspace

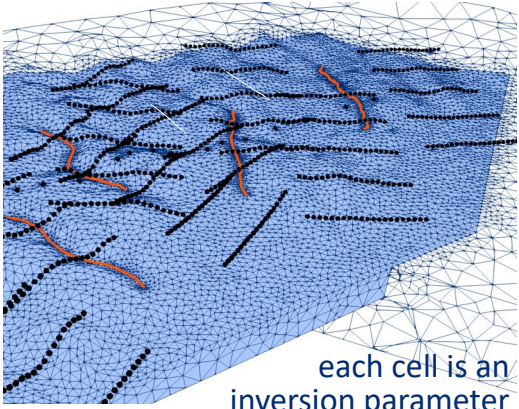

each cell is an inversion parameter

Synthetic 3D large-scale semi-airborne model with real topography

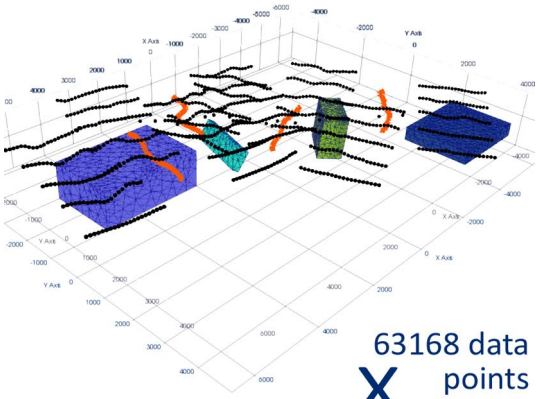

- Anomaly 1 (purple):
  - large resistive brick 5000 Ωm
- Anomaly 2 (cyan):
  - very conductive tiny plate 10 Ωm
- Anomaly 3 (green):
  - conductive larger surface dyke 50 Ωm
- Anomaly 4 (blue):
  - flat semi-conductive brick 200 Ωm
- 4 × 210 full Bx/By/Bz airborne Rx
- Ex/Ey ground stations recording from all Tx
- 12 frequencies between 6 and 3500 Hz
- Gaussian noise: 5%

Inversion result considering topography ...

final resistivity model, real topography

$$\chi^2 = 1.37$$

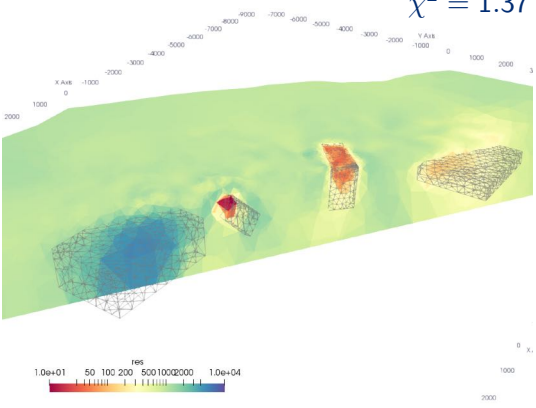

Inversion result considering topography . . . or not

final resistivity model, real topography

$\chi^2 = 1.37$

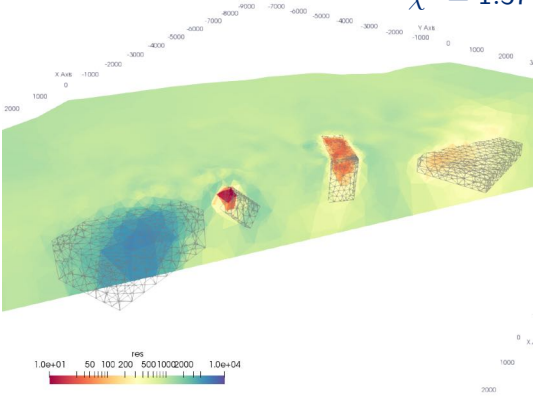

final resistivity model, flat topography

$\chi^2 = 13.12$

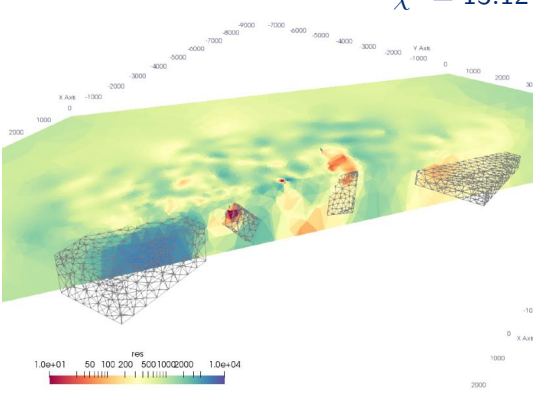

Inversion of synthetic data with and without topography

10 - 50 Ωm, real topography

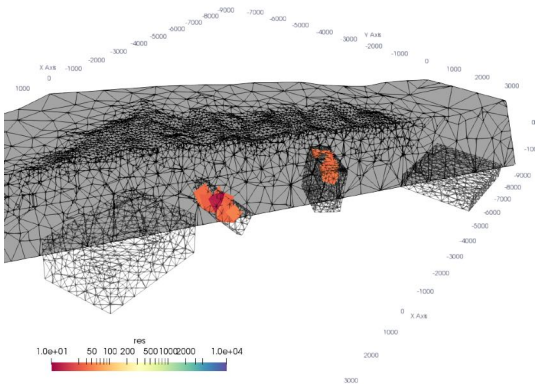

10 - 50 Ωm, flat topography

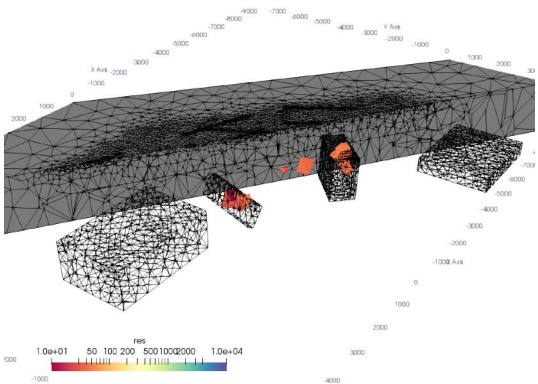

Inversion of synthetic data with and without topography

10 - 100 Ωm, real topography

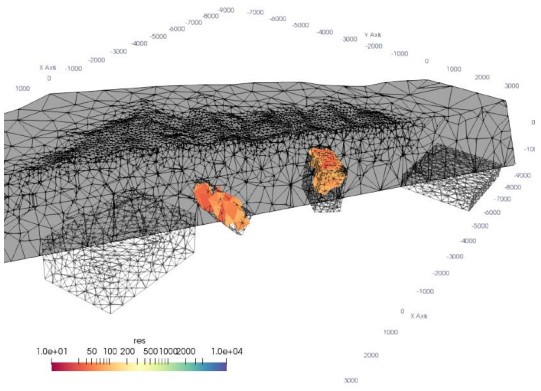

10 - 100 Ωm, flat topography

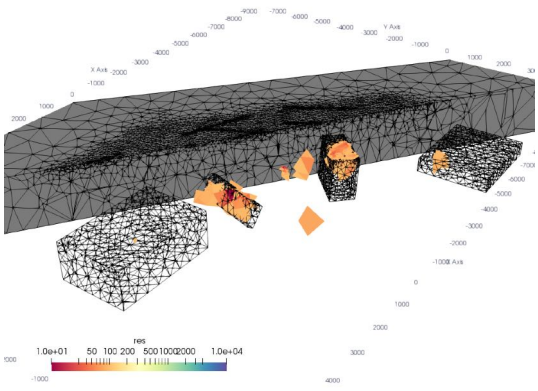

Inversion of synthetic data with and without topography

10 - 250 Ωm, real topography

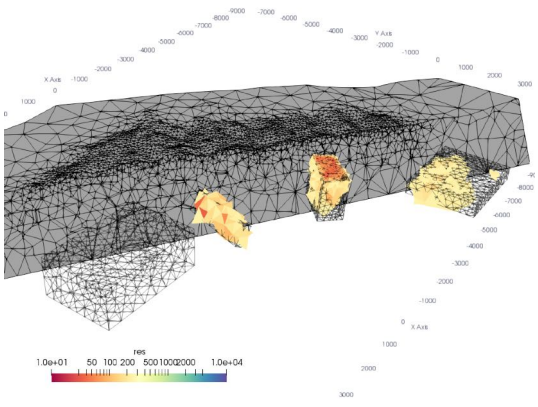

10 - 250 Ωm, flat topography

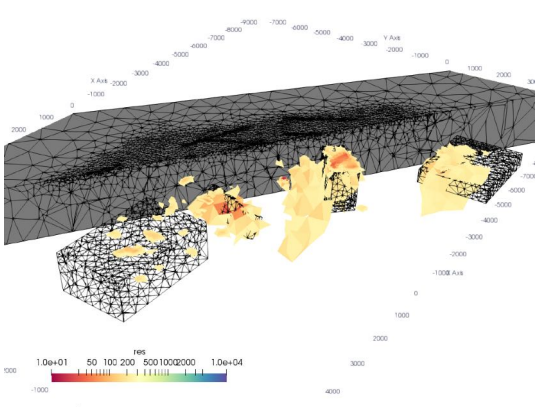

Inversion of synthetic data with and without topography

<250 & >2000 Ωm, real topography

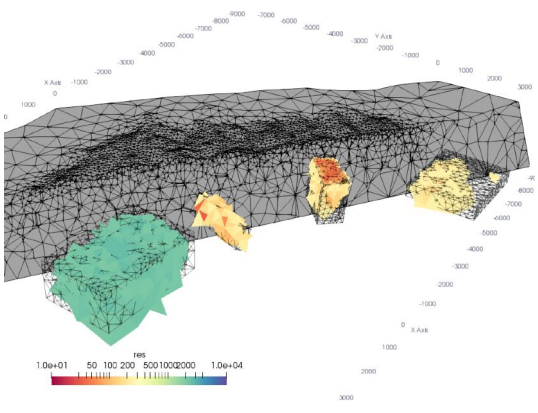

<250 & >2000 Ωm, flat topography

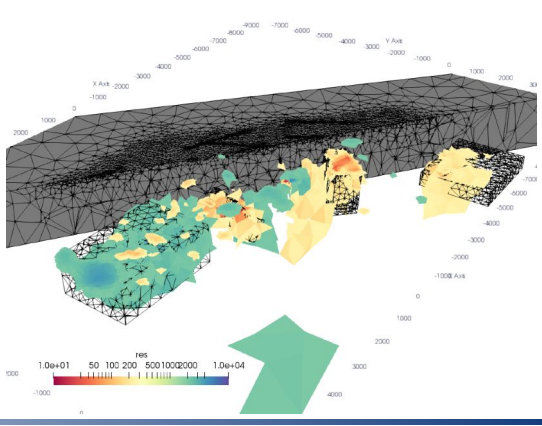

Inversion of semi-airborne Schleiz field data

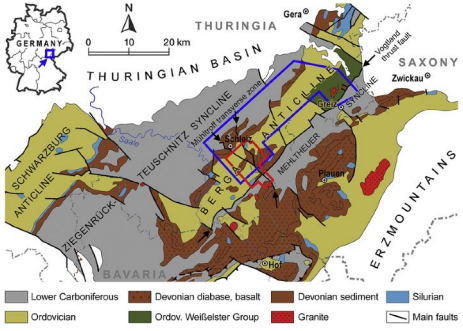

First analysis: Smirnova et al. (2019)
Updated processing: Becken et al. (2020)
Method comparison: Steuer et al. (2020)

Inversion of semi-airborne Schleiz field data

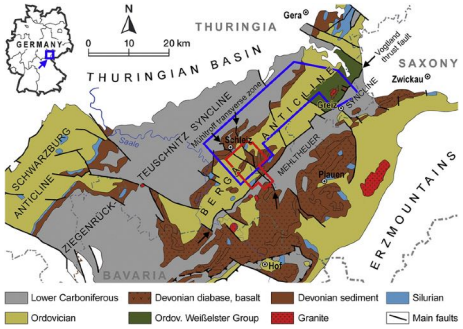

First analysis: Smirnova et al. (2019)
Updated processing: Becken et al. (2020)
Method comparison: Steuer et al. (2020)

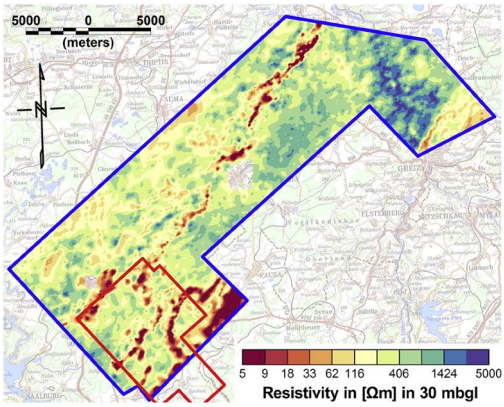

Airborne EM data (Resolve system)

Inversion of semi-airborne Schleiz field data

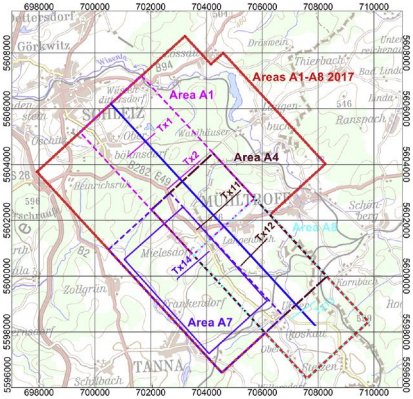

Combined interpretation: Steuer et al. (2020)

Inversion of semi-airborne Schleiz field data

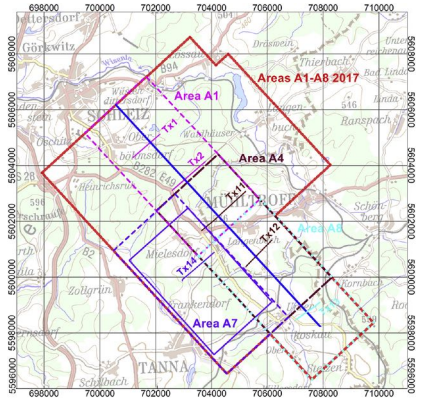

Combined interpretation: Steuer et al. (2020)

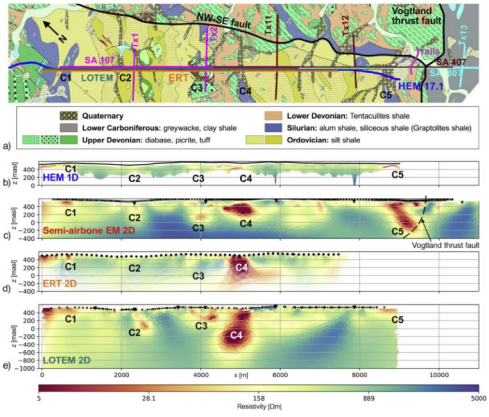

Inversion results on main profile

Data subset for first comparisons

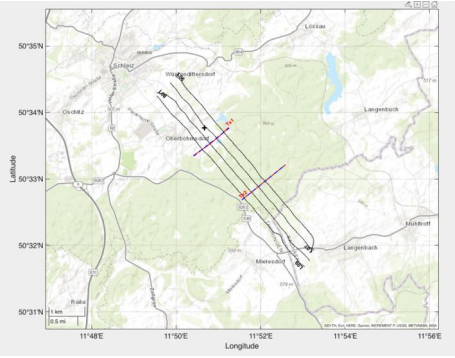

Data subset for first comparisons

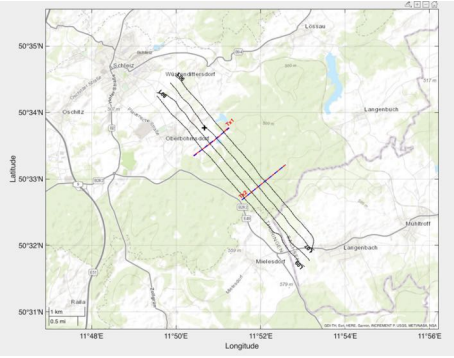

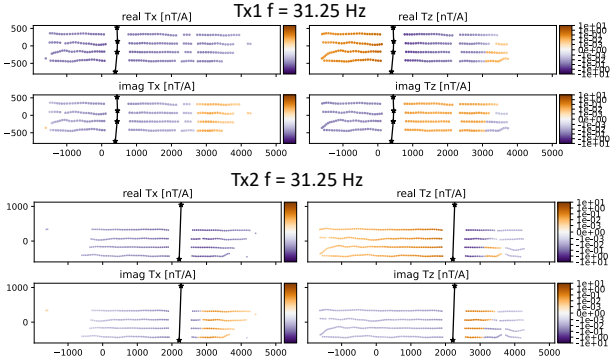

2.5D Mare2DEM vs. custEM 3D inversion

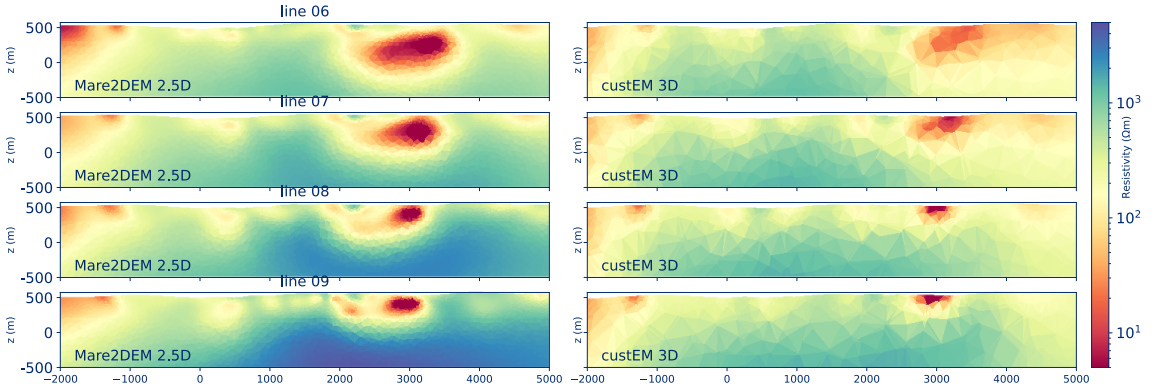

- Data processing and Mare2DEM inversion: M. Becken
- 10 frequencies between 22 and 1090 Hz, error model: 5 % + 1.5 pT/A

2.5D Mare2DEM vs. custEM 2.5D vs. 3D inversion

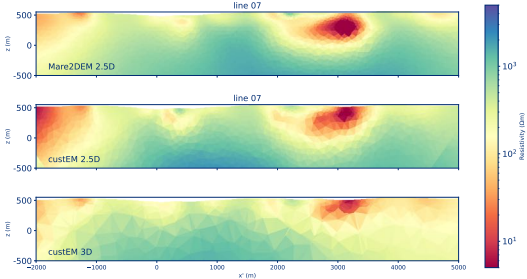

χ^2 development: 2.5D inversion

```
iteration 0 : 67.149
iteration 1 : 25.235
iteration 2 : 16.880
iteration 3 : 11.352
iteration 4 : 6.985
iteration 6 : 4.685
iteration 8 : 3.730
```

χ^2 development: 3D inversion

```
iteration 0 : 149.02
iteration 1 : 38.006
iteration 3 : 10.014
iteration 5 : 5.147
iteration 7 : 2.861
iteration 9 : 2.281
iteration 11: 2.074
```

2.5D Mare2DEM vs. custEM 2.5D vs. 3D inversion

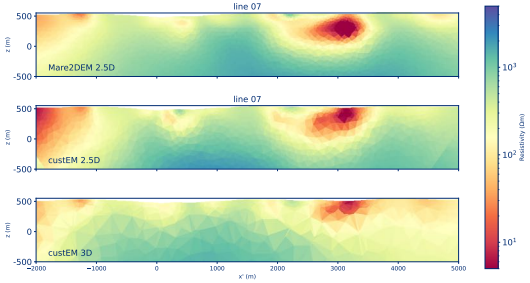

χ^2 development: 2.5D inversion

```
iteration 0 : 67.149
iteration 1 : 25.235
iteration 2 : 16.880
iteration 3 : 11.352
iteration 4 : 6.985
iteration 6 : 4.685
iteration 8 : 3.730
```

χ^2 development: 3D inversion

```
iteration 0 : 149.02
iteration 1 : 38.006
iteration 3 : 10.014
iteration 5 : 5.147
iteration 7 : 2.861
iteration 9 : 2.281
iteration 11: 2.074
```

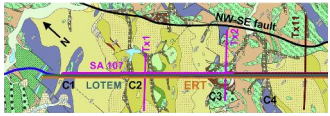

3D view of custEM inversion result

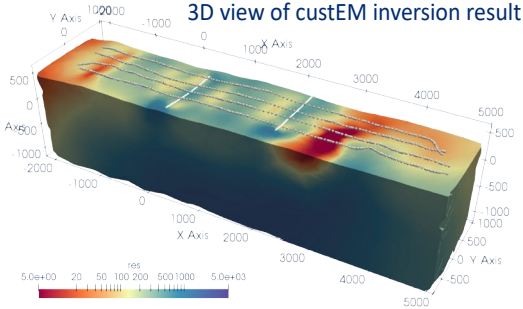

How expensive is it?

How expensive is it?

Table: Computational statistics of presented custEM 3D inversions

example	nodes	n_cpu	t total	RAM total	t / iter	t_fwd	t_bsub	t_inv
Synthetic	50 k	60	44 h	1.2 TB	5.5 h	20 min	≈4 h	80 min
Schleiz 3D	20 k	60	8 h	0.4 TB	40 min	3 min	≈30 min	7 min

How expensive is it?

Table: Computational statistics of presented custEM 3D inversions

example	nodes	n_cpu	t total	RAM total	t / iter	t_fwd	t_bsub	t_inv
Synthetic	50 k	60	44 h	1.2 TB	5.5 h	20 min	≈4 h	80 min
Schleiz 3D	20 k	60	8 h	0.4 TB	40 min	3 min	≈30 min	7 min

- Massive back-substitution time: many N_{obs} for semi-airborne (e.g., 5000/f for synthetic)
- 2.5D inversion has currently massive algebra overhead (can be reduced in future)
- Currently, inverse solver of pyGIMLi is not parallelized

Outlook - Inversion

- Extend implementation of pyGIMLi/custEM CSEM data inversion framework
- Better error models for inverting Helicopter- and UAV-based semi-airborne data sets
- Use explicit Jacobi for resolution analysis
- Add capabilities for combined inversion of EM data sets (CSEM/TEM/MT)
- Test options to speed up inversion of very big data sets by a few factors
- Alternative inversion strategies
- Provide inversion examples to EM community

custEM - Overview

discretization

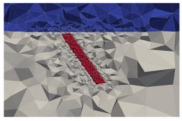

TetGen

A Quality Tetrahedral Mesh Generator and 3D Delaunay Triangulator

https://www.wias-berlin.de/software/tetgen/

pyGIMLi

Geophysical Inversion & Modelling Library

https://www.pygimli.org/

weak formulation / assemble FE system

$$\nabla \times \mu^{-1} \nabla \times \mathbf{E} + i\omega\sigma\mathbf{E} = -i\omega\mathbf{j_e}$$

FEniCS Project

2019.1.0

COMET

solve SLE

sparse, ill-conditioned, symmetric SLE

PETSc

MUMPS

Post-processing

custEM - Source code and documentation

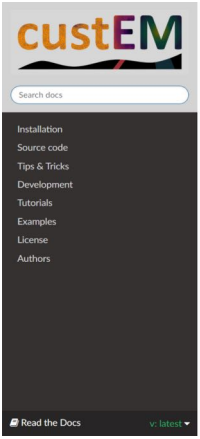

Docs » Welcome to custEM! Edit on GitLab

Welcome to custEM!

Version: 1.2. – Date: Mar 03, 2022

The Python toolbox **custEM** is an open-source development for customizable 3D finite-element modeling of controlled-source, transient, and natural-source electromagnetic data. The toolbox is based on the finite-element library FEniCS, see https://fenicsproject.org/ . Different total and secondary electric or magnetic field as well as gauged-potential approaches are implemented. In addition, **custEM** contains a mesh generation submodule for the straightforward generation of tetrahedral meshes supporting a large number of marine, land-based, airborne or mixed model scenarios. Interpolation and visualization tools simplify the post-processing workflow.

Mesh generation runs on any laptop or desktop PC. Also minimalistic examples can be tested on such machines. Because of using direct solvers, we recommend to get access to a cluster with >= 32 cores/threads and >=256 GB RAM for calculating sufficiently accurate models for more complex 3D setups. However, quite good results for simpler 3D modeling studies often require only 32-64 GB.

Please note that custEM is under continuous development. For information about planned updates and previous development steps we refer to the Development section. Do not hesitate to contact raphael.rochlitz@leibniz-liag.de for any kind of question about custEM or discovered issues in the code, examples, or the documentation.

https://gitlab.com/Rochlitz.R/custEM

https://custem.readthedocs.io

custEM - Examples

fd_e1_hed_1d	15.03.2022 16:31
fd_e2_crooked_loop_1d	12.03.2022 16:43
fd_e3_approach_comparison_3d	15.03.2022 16:31
fd_e4_syth_topo_plate_3d	01.03.2022 11:54
fd_e5_ip_1d	01.03.2022 12:44
mt_e1_dublin_3d	03.03.2022 18:16
td_e1_loop_r_1d	01.03.2022 17:48
td_e2_lotem_3d	12.03.2022 13:55
td_e3_marlim_marine_3d	12.03.2022 14:36
README.rst	01.03.2022 13:54

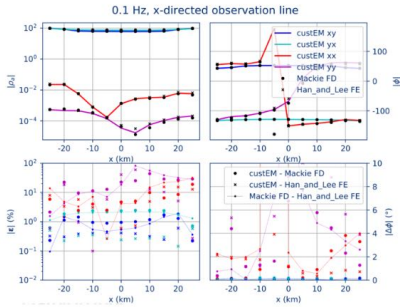

Can be downloaded from: `https://gitlab.com/Rochlitz.R/custEM`

custEM - Installation and requirements

Installation (Unix system)

- Visit: `https://custem.readthedocs.io/en/latest/install.html`
- Default: conda create $-$ n custEM custem

Requirements

- Toy problems: 4 cores and 32 GB RAM
- Modeling studies: $\geq$16 cores and $\geq$128 GB RAM
- Real-world problems / 3D inversion: $\geq$64 cores and $\geq$1TB RAM

Code handling - mesh generation

```
from custEM.meshgen import meshgen_utils as mu
from custEM.meshgen.meshgen_tools import BlankWorld

# %% define Tx
dipole_tx = mu.line_y(start=-5e2, stop=5e2, n_segs=21)
loop_tx = mu.loop_r([-5e2, -5e2], [5e2, 5e2], n_segs=80)

# %% add Rx refinements
rx_tri = mu.refine_rx(mu.line_x(start=-5e3, stop=5e3,
                                n_segs=200), r=10.)

# %% build halfspace or layered earth mesh
M = BlankWorld(name='example_3_mesh_p2',
               preserve_edges=True)

M.build_surface(insert_line_tx=[dipole_tx],
                insert_loop_tx=[loop_tx],
                insert_paths=rx_tri)

M.build_halfspace_mesh()

# %% add anomalies
M.add_plate(x_dim=1000., y_dim=1000., z_dim=100.,
            origin=[500., 100., -700.],
            dip=45., dip_azimuth=117., cell_size=1e4)

# %% call TetGen
M.call_tetgen(tet_param='-pq1.6aA')
```

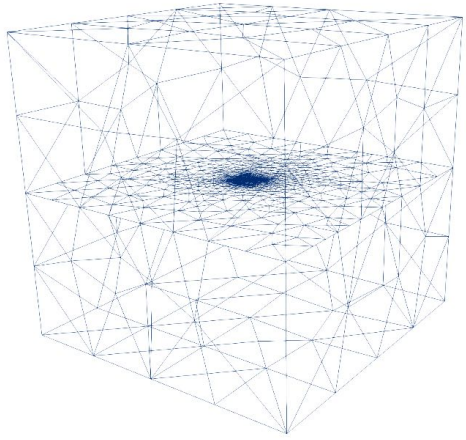

Code handling - run parallel simulation (*"mpirun -n NCORES python MYSCRIPT"*)

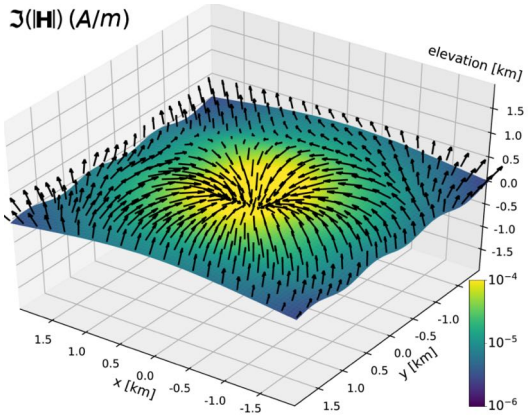


```
import numpy as no
from custEM.core import MOD

# %% initialize model instance
M = MOD('MOD_NAME', 'MESH_NAME', 'E_t', p=2)
```

Change approach -> change EM method (e.g., 'E_IE', 'MT')

```
# %% define frequency and condcutivities
M.MP.update_model_parameters(
        frequencies=np.logspace(1, 3, 3),
        sigma_ground=[1e-3, 1e-2, 1e-4])

# %% do finite element stuff
M.FE.build_var_form()

# %% call solver and convert H-fields
M.solve_main_problem()

# %% manual interpolation
M.IB.create_slice_mesh('z', dim=4000., n_segs=100,
                       slice_name='surface')

# interpolate fields on the observation slice
M.IB.interpolate('surface_slice_z')
```

Code handling - current workflow for inversion

```
import numpy as np
import pygimli as pg
from custEM.meshgen.invmesh_tools import BlankWorld
from custEM.inv.inv_utils import MultiFWD

# %% import data
data = np.load('saemdata.npy')

# %% initialize model instance
M = BlankWorld('invmesh', ...)
...
M.add_inv_domains(...)
...

# %% set up forward operator
fop = MultiFWD('invmod', 'invmesh', n_cores=60,
               inv_type='cells', p_fwd=2)
fop.setRegionProperties("*", limits=[1e-4, 1])

# %% set up inverse operator
inv = pg.Inversion()
inv.setForwardOperator(fop)
inv.dataTrans = pg.trans.TransSymLog(1e-3)
invmodel = inv.run(data.measured, data.errors,
                   lam=100., startModel=1e-3,
                   maxIter=21, verbose=True)
```

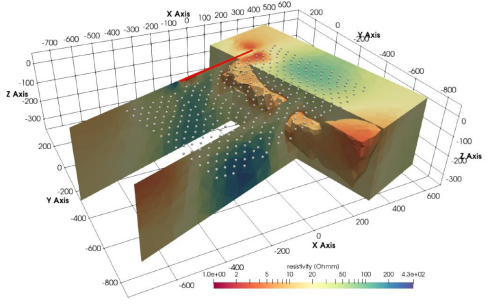

Outlook - the future of custEM?

- Make custEM successively independent of "Rochlitz"
- Share responsibilities, someone interested in Co-developing?
- Implement more features (only possible with Co-developers)
  - mesh design,
  - iterative solvers,
  - adaptive refinement,
  - other inversion methods
- Transition to new FEniCS-X development
- Try to get funding for sustainable software developments

Summary - Why open-source?

Pro open-source arguments

- easier access for others
- guaranteed reproducible
- less redundancy
- more innovation
- easier debugging

Summary - Why open-source?

Pro open-source arguments

- easier access for others
- guaranteed reproducible
- less redundancy
- more innovation
- easier debugging
- simplifies networking

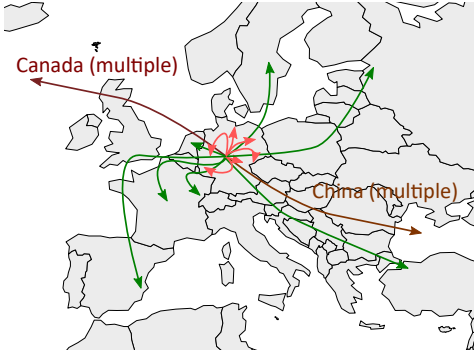

Model comparisons / knowledge exchange with custEM (CSEM, TEM, MT, IP, Aniso)

Acknowledgements

Thomas Günther

Dieter Werthmüller

Nico Skibbe

Ralph-Uwe Börner

Marc Seidel

Michael Becken

Feiyan Wang

Francois Bretaudeau

Markus Schiffler

and many others for comparing models and fruitful discussions.

DESMEX consortium

The developers of FEniCS, pyGIMLi and TetGen

Leibniz Institute for Applied Geophysics

DESMEX

FONA Research for Sustainable Development BMBF

Federal Ministry of Education and Research

Performance of custEM - very problem-dependent

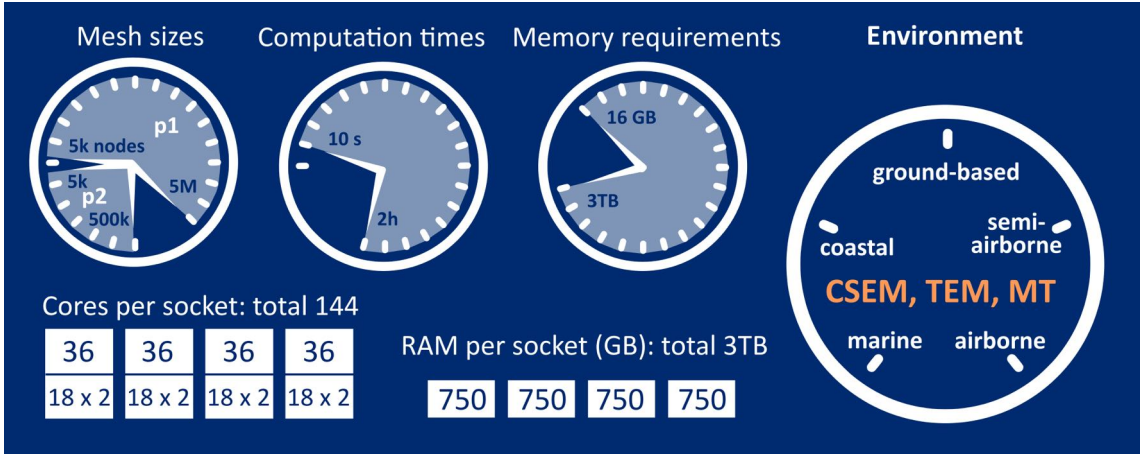

Accuracy of first and second order polynomials

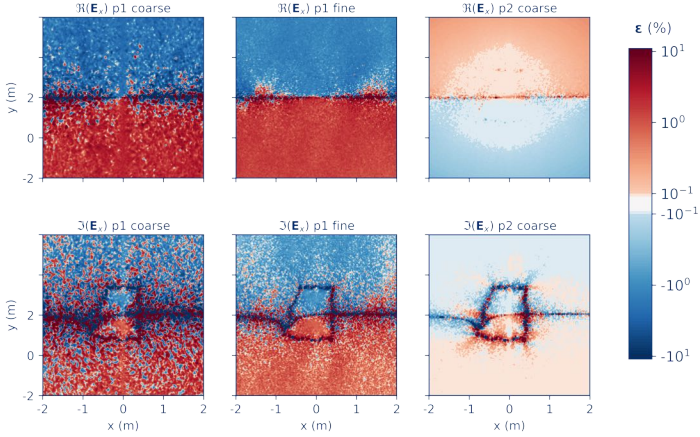

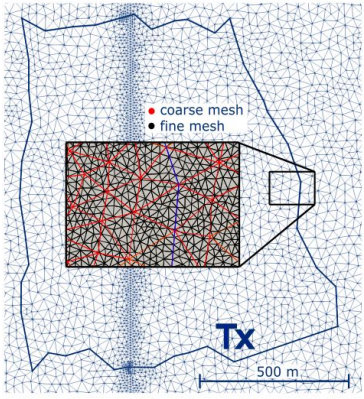

IP modeling - 1D validation (Pelton model)

3 layer model geometry

layer 1:	σ=0.01 S/m	c=0.8	m=0.7	τ=1.
layer 2:	σ=0.1 S/m	c=1.	m=0.5	τ=0.1
layer 3:	σ=0.001 S/m	c=0.	m=0.	τ=0.

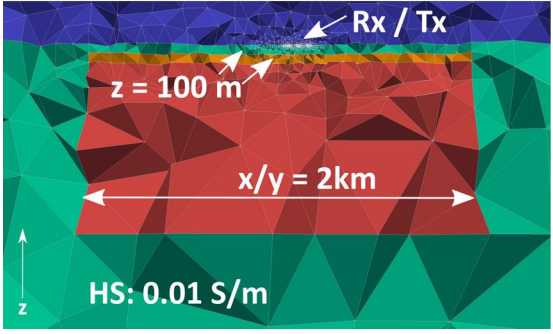

surface view

Tx 1: 200 m dipole (y), center @ x = -200 m
Tx 2: 200 m x 200 m loop witch center @ x = -200 m, y = 0 m

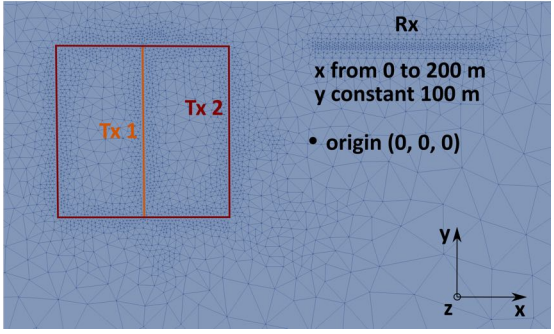

IP modeling - E-field component for dipole source - reference @ empymod (D. Werthmüller)

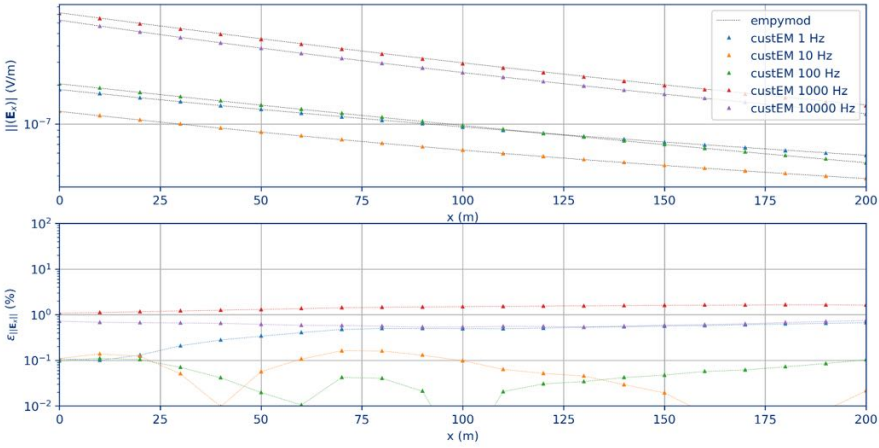

IP modeling - H-field component for loop source - reference @ empymod (D. Werthmüller)

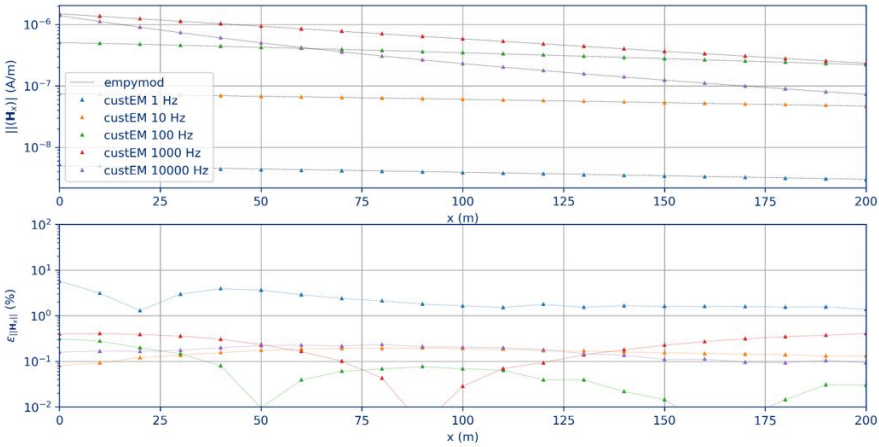

Influence of polynomial order on matrix characteristics

Table: Matrix characteristics dependent on approach (appr.) and polynomial order (p) for regular UnitCubeMesh and irregular CSEM modeling mesh; matrix size (s), number of non-zero entries (nz), minimum l_{min} and maximum l_{max} non-zero entries per row.

		Regular mesh				Irregular mesh			
nodes / elements		1331 / 6000				1286 / 7371			
edge lengths (m)		min.: 1000 / max.: 1732				min.: 1. / max.: 5000			
appr.	p	s (k)	nz (M)	l_{min}	l_{max}	s (k)	nz (M)	l_{min}	l_{max}
E, H	1	15.9	0.46	12	38	17.6	0.57	11	68
E, H	2	82.1	6.77	40	148	94.9	8.19	39	268
E, H	3	235	38.6	90	366	276	46.9	89	666

Parallel computational performance for layered-earth model

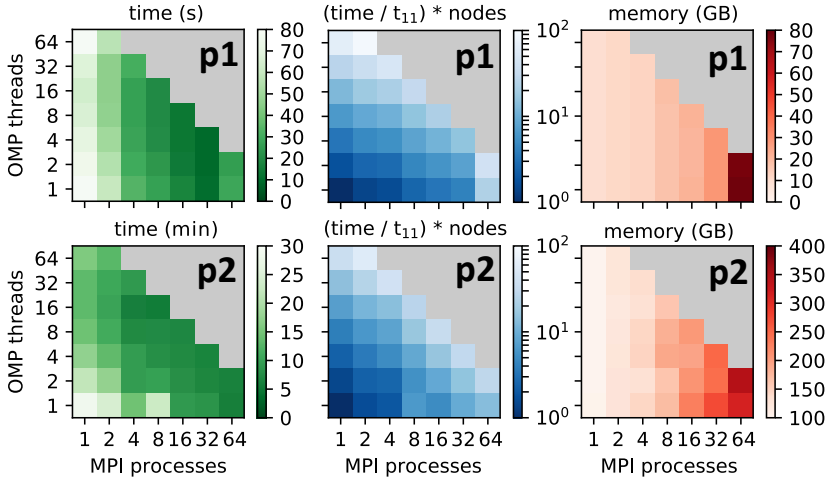

Effects of topography on semi-airborne data

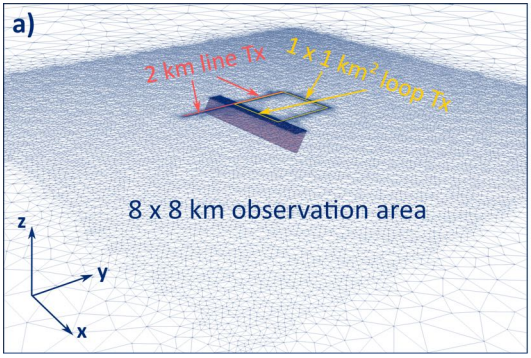

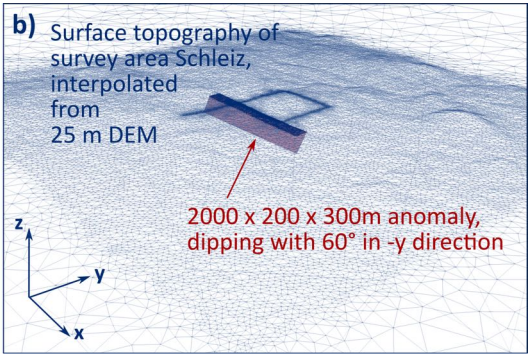

Effects of topography on semi-airborne data

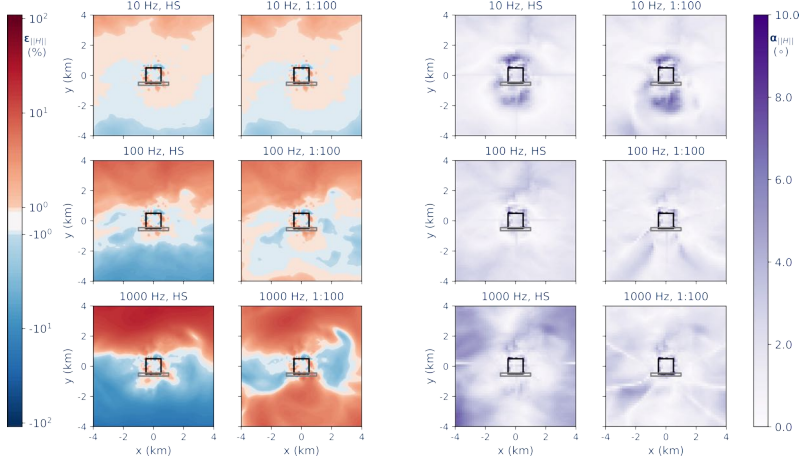

Very challenging EM models - Etang de Thau

Issues

- Water depths $< 10\,\mathrm{m}$ over several km^2,
- highly conductive water: $0.18\,\Omega\mathrm{m}$,
- Smoothing of digital elevation model,
- Sufficient extent of real geometry,
- Avoid tremendous amount of elements by using a water layer with equivalent conductance?

Very challenging EM models - Etang de Thau

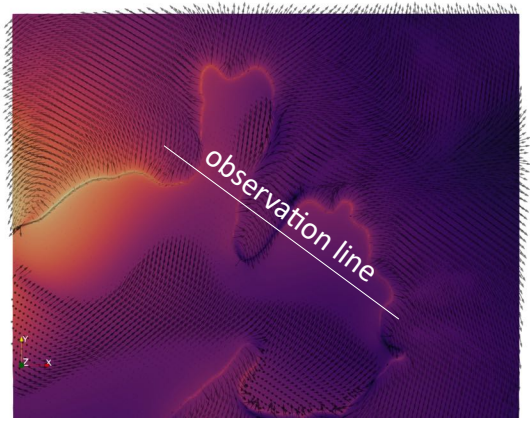

Reference @ Francois Bretaudeau (POLYEM3D)

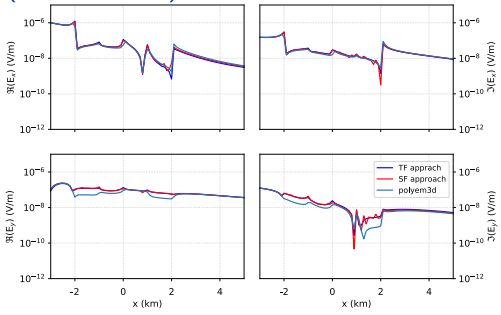

References I

Adhidjaja, J. I. and Hohmann, G. W. (1989). A finite-difference algorithm for the transient electromagnetic response of a three-dimensional body, *Geophysical Journal International* **98**(2): 233–242.

Alumbaugh, D. L., Newman, G. A., Prevost, L. and Shadid, J. N. (1996). Three-dimensional wideband electromagnetic modeling on massively parallel computers, *Radio Science* **31**(1): 1–23.

Ansari, S. (2014). *Three dimensional finite-element numerical modeling of geophysical electromagnetic problems using tetrahedral unstructured grids*, PhD thesis, Memorial University of Newfoundland.

Ansari, S. and Farquharson, C. G. (2014). 3D finite-element forward modeling of electromagnetic data using vector and scalar potentials and unstructured grids, *Geophysics* **79**(4): E149–E165.

Badea, E. A., Everett, M. E., Newman, G. A. and Biro, O. (2001). Finite-element analysis of controlled-source electromagnetic induction using coulomb-gauged potentials, *Geophysics* **66**(3): 786–799.

Becken, M., Nittinger, C. G., Smirnova, M., Steuer, A., Martin, T., Petersen, H., Meyer, U., Mörbe, W., Yogeshwar, P., Tezkan, B. et al. (2020). Desmex: A novel system development for semi-airborne electromagnetic exploration, *Geophysics* **85**(6): E253–E267.

Biro, O. and Preis, K. (1989). On the use of the magnetic vector potential in the finite-element analysis of three-dimensional eddy currents, *IEEE Transactions on magnetics* **25**(4): 3145–3159.

Börner, R.-U., Ernst, O. G. and Güttel, S. (2015). Three-dimensional transient electromagnetic modelling using rational Krylov methods, *Geophysical Journal International* **202**(3): 2025–2043.

Bretaudeau, F., Penz, S., Coppo, N., Wawrzyniak, P. and Darnet, M. (2017). Practical inversion of electric resistivity in 3d from frequency-domain land csem data, *23rd European Meeting of Environmental and Engineering Geophysics*, Vol. 2017, European Association of Geoscientists & Engineers, pp. 1–5.

Cai, H., Hu, X., Xiong, B., Auken, E., Han, M. and Li, J. (2017). Finite element time domain modeling of controlled-source electromagnetic data with a hybrid boundary condition, *Journal of Applied Geophysics* **145**: 133–143.

References II

Cai, H., Xiong, B., Han, M. and Zhdanov, M. (2014). 3D controlled-source electromagnetic modeling in anisotropic medium using edge-based finite element method, *Computers & Geosciences* **73**: 164–176.

Castillo-Reyes, O., de la Puente, J. and Cela, J. M. (2018). PETGEM: A parallel code for 3D CSEM forward modeling using edge finite elements, *Computers & Geosciences* **119**: 123–136.

Cockett, R., Kang, S., Heagy, L. J., Pidlisecky, A. and Oldenburg, D. W. (2015). SimPEG: An open source framework for simulation and gradient based parameter estimation in geophysical applications, *Computers & Geosciences* **85**: 142–154.

Coggon, J. (1971). Electromagnetic and electrical modeling by the finite element method, *Geophysics* **36**(1): 132–155.

Commer, M. and Newman, G. (2004). A parallel finite-difference approach for 3D transient electromagnetic modeling with galvanic sources, *Geophysics* **69**(5): 1192–1202.

Correa, J. L. and Menezes, P. T. (2019). Marlim R3D: A realistic model for controlled-source electromagnetic simulations-phase 2: The controlled-source electromagnetic data set, *Geophysics* **84**(5): E293–E299.

Da Silva, N. V., Morgan, J. V., MacGregor, L. and Warner, M. (2012). A finite element multifrontal method for 3D CSEM modeling in the frequency domain, *Geophysics* **77**(2): E101–E115.

Druskin, V. L. and Knizhnerman, L. (1988). Spectral differential-difference method for numeric solution of three-dimensional nonstationary problems of electric prospecting, *Earth Physics* **24**(8): 641–648.

Egbert, G. D. and Kelbert, A. (2012). Computational recipes for electromagnetic inverse problems, *Geophysical Journal International* **189**(1): 251–267.

Farquharson, C. G. and Miensopust, M. P. (2011). Three-dimensional finite-element modelling of magnetotelluric data with a divergence correction, *Journal of Applied Geophysics* **75**(4): 699–710.

Grayver, A. V. and Bürg, M. (2014). Robust and scalable 3-D geo-electromagnetic modelling approach using the finite element method, *Geophysical Journal International* **198**(1): 110–125.

References III

Grayver, A. V., Streich, R. and Ritter, O. (2013). Three-dimensional parallel distributed inversion of csem data using a direct forward solver, *Geophysical Journal International* **193**(3): 1432–1446.

Grayver, A. V., van Driel, M. and Kuvshinov, A. V. (2019). Three-dimensional magnetotelluric modelling in spherical earth, *Geophysical Journal International* **217**(1): 532–557.

Gupta, P., Raiche, A. and Sugeng, F. (1989). Three-dimensional time-domain electromagnetic modelling using a compact finite-element frequency-stepping method, *Geophysical Journal International* **96**(3): 457–468.

Haber, E., Ascher, U., Aruliah, D. and Oldenburg, D. (2000). Fast simulation of 3D electromagnetic problems using potentials, *Journal of Computational Physics* **163**(1): 150–171.

Haber, E., Ascher, U. and Oldenburg, D. W. (2002). 3d forward modelling of time domain electromagnetic data, *SEG Technical Program Expanded Abstracts 2002*, Society of Exploration Geophysicists, pp. 641–644.

Hohmann, G. W. (1975). Three-dimensional induced polarization and electromagnetic modeling, *Geophysics* **40**(2): 309–324.

Hohmann, G. W. (1983). Three-dimensional em modeling, *Geophysical Surveys* **6**(1-2): 27–53.

Jahandari, H. and Farquharson, C. G. (2014). A finite-volume solution to the geophysical electromagnetic forward problem using unstructured grids, *Geophysics* **79**(6): E287–E302.

Kelbert, A., Meqbel, N., Egbert, G. D. and Tandon, K. (2014). Modem: A modular system for inversion of electromagnetic geophysical data, *Computers & Geosciences* **66**: 40–53.

Key, K. (2016). Mare2dem: a 2-D inversion code for controlled-source electromagnetic and magnetotelluric data, *Geophysical Journal International* **207**(1): 571–588.

Kordy, M., Cherkaev, E. and Wannamaker, P. (2017). Null space correction and adaptive model order reduction in multi-frequency Maxwell's problem, *Advances in Computational Mathematics* **43**(1): 171–193.

References IV

Kruglyakov, M., Geraskin, A. and Kuvshinov, A. (2016). Novel accurate and scalable 3-D MT forward solver based on a contracting integral equation method, *Computers & Geosciences* **96**: 208–217.

Li, J., Farquharson, C. G. and Hu, X. (2016a). 3D vector finite-element electromagnetic forward modeling for large loop sources using a total-field algorithm and unstructured tetrahedral grids, *Geophysics* **82**(1): E1–E16.

Li, J., Farquharson, C. G. and Hu, X. (2016b). Three effective inverse Laplace transform algorithms for computing time-domain electromagnetic responses, *Geophysics* **81**(2): E113–E128.

Livelybrooks, D. (1993). Program 3Dfeem: a multidimensional electromagnetic finite element model, *Geophysical Journal International* **114**(3): 443–458.

Mackie, R. L. and Madden, T. R. (1993). Three-dimensional magnetotelluric inversion using conjugate gradients, *Geophysical Journal International* **115**(1): 215–229.

Madden, T. and Mackie, R. L. (1989). Three-dimensional magnetotelluric modelling and inversion, *Proceedings of the IEEE* **77**(2): 318–333.

Miensopust, M. P. (2017). Application of 3-D electromagnetic inversion in practice: Challenges, pitfalls and solution approaches, *Surveys in Geophysics* **38**(5): 869–933.

Mitsuhata, Y. and Uchida, T. (2004). 3D magnetotelluric modeling using the T-Ω finite-element method, *Geophysics* **69**(1): 108–119.

Mukherjee, S. and Everett, M. E. (2011). 3D controlled-source electromagnetic edge-based finite element modeling of conductive and permeable heterogeneities, *Geophysics* **76**(4): F215–F226.

Pridmore, D., Hohmann, G., Ward, S. and Sill, W. (1981). An investigation of finite-element modeling for electrical and electromagnetic data in three dimensions, *Geophysics* **46**(7): 1009–1024.

Puzyrev, V., Koldan, J., de la Puente, J., Houzeaux, G., Vázquez, M. and Cela, J. M. (2013). A parallel finite-element method for three-dimensional controlled-source electromagnetic forward modelling, *Geophysical Journal International* **193**(2): 678–693.

Raiche, A. (1974). An integral equation approach to three-dimensional modelling, *Geophysical Journal International* **36**(2): 363–376.

References V

Ren, Z., Kalscheuer, T., Greenhalgh, S. and Maurer, H. (2013). A goal-oriented adaptive finite-element approach for plane wave 3-D electromagnetic modelling, *Geophysical Journal International* **194**(2): 700–718.

Rochlitz, R. (2020). *Analysis and open-source Implementation of Finite Element Modeling techniques for Controlled-Source Electromagnetics*, PhD thesis, Westfälische Wilhelms-Universität Münster.

Rochlitz, R., Seidel, M. and Börner, R.-U. (2021). Evaluation of three approaches for simulating 3-d time-domain electromagnetic data, *Geophysical Journal International* **227**(3): 1980–1995.

Rochlitz, R., Skibbe, N. and Günther, T. (2019). custEM: Customizable finite-element simulation of complex controlled-source electromagnetic data, *Geophysics* **84**(2): F17–F33.

Rodi, W. L. (1976). A technique for improving the accuracy of finite element solutions for magnetotelluric data, *Geophysical Journal International* **44**(2): 483–506.

Rücker, C., Günther, T. and Wagner, F. (2017). pyGIMLi: An open-source library for modelling and inversion in geophysics, *Computers & Geosciences* **109**: 106–123.

Rulff, P., Buntin, L. M. and Kalscheuer, T. (2021). Efficient goal-oriented mesh refinement in 3-D finite-element modelling adapted for controlled source electromagnetic surveys, *Geophysical Journal International* **227**(3): 1624–1645.

SanFilipo, W. A. and Hohmann, G. W. (1985). Integral equation solution for the transient electromagnetic response of a three-dimensional body in a conductive half-space, *Geophysics* **50**(5): 798–809.

Schwarzbach, C. (2009). *Stability of Finite Element Solutions to Maxwell's Equations in Frequency Domain*, PhD thesis, TU Bergakademie Freiberg, Germany.

Schwarzbach, C., Börner, R.-U. and Spitzer, K. (2011). Three-dimensional adaptive higher order finite element simulation for geo-electromagnetics – a marine CSEM example, *Geophysical Journal International* **187**(1): 63–74.

Siripunvaraporn, W. and Egbert, G. (2009). Wsinv3dmt: vertical magnetic field transfer function inversion and parallel implementation, *Physics of the Earth and Planetary Interiors* **173**(3-4): 317–329.

References VI

Siripunvaraporn, W., Egbert, G. and Lenbury, Y. (2002). Numerical accuracy of magnetotelluric modeling: a comparison of finite difference approximations, *Earth, planets and space* **54**(6): 721–725.

Slob, E. C., van den Berg, P. M., Oristaglio, M. and Spies, B. (1999). Integral-equation method for modeling transient diffusive electromagnetic scattering, *Three-dimensional electromagnetics: SEG* pp. 42–58.

Smirnova, M. V., Becken, M., Nittinger, C., Yogeshwar, P., Mörbe, W., Rochlitz, R., Steuer, A., Costabel, S., Smirnov, M. Y. and Group, D. W. (2019). A novel semiairborne frequency-domain controlled-source electromagnetic system: Three-dimensional inversion of semiairborne data from the flight experiment over an ancient mining area near Schleiz, Germany, *Geophysics* **84**(5): E281–E292.

Stalnaker, J. L. (2005). *A finite element approach to the 3D CSEM modeling problem and applications to the study of the effect of target interaction and topography*, PhD thesis, Texas A&M University.

Steuer, A., Smirnova, M., Becken, M., Schiffler, M., Günther, T., Rochlitz, R., Yogeshwar, P., Moerbe, W., Siemon, B., Costabel, S. et al. (2020). Comparison of novel semi-airborne electromagnetic data with multi-scale geophysical, petrophysical and geological data from Schleiz, Germany, *Journal of Applied Geophysics* **182**: 104172.

Streich, R. (2009). 3D finite-difference frequency-domain modeling of controlled-source electromagnetic data: Direct solution and optimization for high accuracy, *Geophysics* **74**(5): F95–F105.

Tang, W., Li, Y., Swidinsky, A. and Liu, J. (2015). Three-dimensional controlled-source electromagnetic modelling with a well casing as a grounded source: a hybrid method of moments and finite element scheme, *Geophysical Prospecting* **63**(6): 1491–1507.

Ting, S. C. and Hohmann, G. W. (1981). Integral equation modeling of three-dimensional magnetotelluric response, *Geophysics* **46**(2): 182–197.

Um, E. S., Harris, J. M. and Alumbaugh, D. L. (2010). 3D time-domain simulation of electromagnetic diffusion phenomena: A finite-element electric-field approach, *Geophysics* **75**(4): F115–F126.

Um, E. S., Harris, J. M. and Alumbaugh, D. L. (2012). An iterative finite element time-domain method for simulating three-dimensional electromagnetic diffusion in earth, *Geophysical Journal International* **190**(2): 871–886.

References VII

Wang, F., Morten, J. P. and Spitzer, K. (2018). Anisotropic three-dimensional inversion of CSEM data using finite-element techniques on unstructured grids, *Geophysical Journal International* **213**(2): 1056–1072.

Wang, F., Ren, Z. and Zhao, L. (2022). A goal-oriented adaptive finite-element approach for 3-D marine controlled-source electromagnetic problems with general electrical anisotropy, *Geophysical Journal International* **229**(1): 439–458.

Wang, T. and Hohmann, G. W. (1993). A finite-difference, time-domain solution for three-dimensional electromagnetic modeling, *Geophysics* **58**(6): 797–809.

Wannamaker, P. E. (1991). Advances in three-dimensional magnetotelluric modeling using integral equations, *Geophysics* **56**(11): 1716–1728.

Weidelt, P. et al. (1975). Electromagnetic induction in three-dimensional structures.

Werthmüller, D. (2017). An open-source full 3D electromagnetic modeler for 1D VTI media in python: empymod, *Geophysics* **82**(6): WB9–WB19.

Werthmüller, D., Mulder, W. A. and Slob, E. C. (2021). Fast Fourier transform of electromagnetic data for computationally expensive kernels, *Geophysical Journal International* **226**(2): 1336–1347.

Werthmüller, D., Rochlitz, R., Castillo-Reyes, O. and Heagy, L. (2020). Open-source landscape for 3D CSEM modelling, *arXiv preprint arXiv:2010.12926* .

Zhdanov, M. S., Lee, S. K. and Yoshioka, K. (2006). Integral equation method for 3D modeling of electromagnetic fields in complex structures with inhomogeneous background conductivity, *Geophysics* **71**(6): G333–G345.